A highly conserved ligand-binding site for AccA transporters of antibiotic and quorum-sensing regulator in Agrobacterium leads to a different specificity

Solange Moréra, Armelle Vigouroux, Magali Aumont-Nicaise, Mohammed Ahmar, Thibault Meyer, Abbas El Sahili, Grégory Deicsics, Almudena González-Mula, Sizhe Li, Jeanne Doré, et al.

A highly conserved ligand-binding site for AccA transporters of antibiotic and quorum-sensing regulator in *Agrobacterium* leads to a different specificity

Solange Moréra[1]*, Armelle Vigouroux[1], Magali Aumont-Nicaise[1], Mohammed Ahmar[2], Thibault Meyer[3], Abbas El Sahili[1$], Grégory Deicsics[1], Almudena González-Mula[1], Sizhe Li[2], Jeanne Doré[3], Serena Siragu[4], Pierre Legrand[4], Camille Penot[1], François André[1], Denis Faure[1], Laurent Soulère[2], Yves Queneau[2], Ludovic Vial[3]

[1]Université Paris-Saclay, CEA, CNRS, Institute for Integrative Biology of the Cell (I2BC), 91198, Gif-sur-Yvette, France

[2]Univ Lyon, Institut de Chimie et Biochimie Moléculaires et Supramoléculaires, CNRS, Université Lyon 1, INSA Lyon, CPE Lyon, ICBMS, UMR 5246; Université Claude Bernard, Bâtiment Lederer, 69622 Villeurbanne Cedex, France

[3]UMR Ecologie Microbienne, CNRS, INRAE, VetAgro Sup, UCBL, Université de Lyon, F-69622, Villeurbanne, Lyon, France

[4]Synchrotron SOLEIL, HelioBio group, 91190 Saint-Aubin, France

Short title: Specificity of the *Agrobacterium tumefaciens* strain Bo542 for agrocinopine uptake

*Corresponding author: solange.morera@i2bc.paris-saclay.fr; Tel +33 1 69 82 42 13, ORCID ID: 0000-0001-7781-0448

Abstract

Plants genetically modified by the pathogenic *Agrobacterium* strain C58 synthesize agrocinopines A and B, whereas those modified by the pathogenic strain Bo542 produce agrocinopines C and D. The four agrocinopines (A, B, C and D) serve as nutrients by agrobacteria and signaling molecule for the dissemination of virulence genes. They share the uncommon pyranose-2-phosphate motif, represented by the L-arabinopyranose moiety in agrocinopines A/B and the D-glucopyranose moiety in agrocinopines C/D, also found in the antibiotic agrocin 84. They are imported into agrobacterial cytoplasm *via* the Acc transport system, including the solute-binding protein AccA coupled to an ABC transporter. We have previously shown that unexpectedly, AccA from strain C58 (AccAC58) recognizes the pyranose-2-phosphate motif present in all four agrocinopines and agrocin 84, meaning that strain C58 is able to import agrocinopines C/D, originating from the competitor strain Bo542. Here, using agrocinopine derivatives and combining crystallography, affinity and stability measurements, modeling, molecular dynamics, *in vitro* and *vivo* assays, we show that AccABo542 and AccAC58 behave differently despite 75% sequence identity and a nearly identical ligand binding site. Indeed, strain Bo542 imports only compounds containing the D-glucopyranose-2-phosphate moiety, and with a lower affinity compared to strain C58. This difference in import efficiency makes C58 more competitive than Bo542 in culture media. We can now explain why *Agrobacterium/Allorhizobium vitis* strain S4 is insensitive to agrocin 84, although its genome contains a conserved Acc transport system. Overall, our work highlights AccA proteins as a case study, for which stability and dynamics drive specificity.

Keywords: agrocinopine A, agrocinopine D, agrocin 84, solute binding protein AccA, *Agrobacterium tumefaciens* strain Bo542, *Allorhizobium vitis* strain S4, pTi

Introduction

Agrobacterium pathogens possessing a Ti (Tumor inducing) plasmid are responsible for the crown gall disease observed on plants (1, 2). Upon plant infection, a small DNA fragment (T-DNA) from their Ti plasmid is transferred and integrated into the plant nuclear genome leading to genetically modified plant cells and plant-tumor formation, creating an ecological niche (also opine niche) for the agrobacteria (3, 4) (5) (2). Indeed, in *Agrobacterium*-induced plant tumors colonized by agrobacteria, the bacterial T-DNA encodes genes allowing the production of opines, which are used as specific nutrients by agrobacteria, conferring them an advantage when in competition with other bacteria of the soil microflora for the colonization of opine-rich environments (6) (7) (8) (9). Octopine and the pyranose-2-phosphate moiety of agrocinopines (10) are also used as regulatory signals by agrobacteria to induce the horizontal transfer (conjugative transfer) of the pTi from pathogenic *Agrobacterium* to non-pathogenic *Agrobacterium* (11).

Opines are classified into distinct families based on their precursors, which include sugars, amino acids and ketoacids. They are not all simultaneously present or synthesized within a tumor. Their composition varies depending on the specific pTi present in the *Agrobacterium* strain. For instance, *Agrobacterium fabrum* strains C58 and *Agrobacterium tumefaciens* strains Bo542 possess Ti plasmid genes that code for enzymes responsible for synthesizing agrocinopines namely agrocinopines A and B for the strain C58 and agrocinopines C and D for the strain Bo542. Agrocinopines A/C are composed of a sucrose linked to L-arabinose/D-glucose *via* a phosphodiester bond, respectively, and agrocinopines B and D lack one sugar from the sucrose moiety (Figure 1A).

The properties of opine catabolism, including import and degradation, are also determined by genes present on a given pTi. These genes, often organized into operons and regulons, are located outside the T-DNA fragment. Their expression is inducible by the opine itself or its catabolized/degraded form (11) (10) (12) (13). The catabolic region typically contains two sets of genes. The first set encodes the transport system, often comprising an ATP-binding cassette (ABC) transporter and a solute-binding protein (SBP). The second set encodes enzymes responsible for opine degradation into molecules that integrate into the central bacterial metabolism. For example, the Acc transport system encoded by the *acc* (agrocinopine catabolism) operon includes the SBP AccA and its associated ABC transporter (import of agrocinopine), the phosphodiesterase AccF (agrocinopine degradation into L-arabinose-2-phosphate or D-glucose-2-phosphate and sucrose) and the key transcriptional regulator AccR. AccR controls the expression of *acc* operon genes as well as *traR* coding for a transcription factor, using the catabolized forms of agrocinopines, such as the L-arabinose-2-phosphate or D-glucose-2-phosphate as effectors (10). The transcription activator TraR interacts with the quorum-sensing signals promoting the expression of the *tra*, *trb* and *rep* genes. This, in turn, stimulates the biosynthesis of the quorum-sensing signals and amplification of copy number and conjugation of the Ti plasmid.

We have previously characterized the SBP AccA from *A. fabrum* strain C58 (AccAC58) and showed how AccAC58 imports the antibiotic agrocin 84 (Figure 1A), which kills agrobacteria according to the Trojan Horse paradigm (14) (15) (10). Once imported by Acc transport system into agrobacteria, agrocin 84 is maturated by the phosphodiesterase AccF into D-glucose-2-phosphamidate and the toxic moiety TM84, which acts as a tRNA-dependent inhibitor of leucyl-tRNA synthetase preventing tRNA Leu aminoacylation, and thereby halting protein synthesis (16) (5) (17) (15). The antibiotic is produced by the *Rhizobium radiobacter* strain K84 that colonizes the same plant environment as *Agrobacterium* pathogens (18) (19). Moreover, we highlighted that AccAC58 is a gateway allowing the import of any compound possessing a pyranose-2-phosphate motif at one end (10). Here, we

investigated the Acc transport system of agrocinopines in the *A. tumefaciens* strain Bo542 and the structural and biochemical properties of the SBP AccABo542 to compare its ligand specificity with the SBP AccAC58 (Figure 1B) (20). We combined *in vivo* (growth assays) and *in vitro* (crystallography, stability and affinity measurements, modeling, molecular dynamics) approaches using synthetic agrocinopines and analogues (Figure 1A and S1, (10) (21)), and we showed that AccABo542 presents a different selectivity towards these compounds compared to AccAC58, enabling the import of molecules containing only a D-glucose-2-phosphate moiety such as agrocinopines C/D as well as agrocin 84, which contains a close motif with its D-glucose-2-phosphoramidate. Interestingly, amino-acid mutations in the ligand-binding site of AccABo542 that make it resemble AccAC58 did not modify AccABo542 specificity. Being able to easily model a bound L-arabinose-2-phosphate in the ligand-binding site of AccABo542, opens a puzzling question on the accurate molecular mechanism supporting the difference of specificity between both AccA proteins, which share 75% sequence identity.

Besides, we were searching for *Agrobacterium* pathogenic strains insensitive to agrocin 84 and containing an Acc transport system, aiming at discovering an AccA protein specific for agrocinopines A/B. From literature, we found out that *Agrobacterium vitis* strain S4 (nowadays renamed *Allorhizobium vitis*) was a good candidate because it was resistant to agrocin 84 and harbors an *acc* operon displaying 76% sequence identity with that of the strain C58. Moreover, its genome was the first *Agrobacterium vitis* sequenced and available at that time (22). We confirmed that the strain S4 cannot import agrocin 84 and surprisingly, we showed that it could neither assimilate agrocinopines nor derivatives. Using reporter genes and growth assays, we demonstrated that the S4 *acc* operon is located on the chromosome1 - and not on the pTi as expected - and that is not transcribed.

We have extensively characterized AccAS4, AccAC58 and AccABo542 to find out the key elements of ligand specificity. AccAS4, AccAC58 and AccABo542 display between 70 and 90% sequence identity. While inspection of the numerous AccA structures did not provide any evidence, molecular dynamics and protein stability brought some clues.

Results

Strains Bo542 and LBA288 (C58pTiBo542) grow only on molecules containing D-glucose-2-phosphate moiety inducing quorum-sensing signal and conjugation. The growth profiles of *A. fabrum* C58 (containing pTiC58) and *A. tumefaciens* Bo542 (containing pTiBo542) were compared in minimal medium including succinate (as control), L-arabinose-2-phosphate, D-glucose-2-phosphate, agrocinopine A or agrocinopine D-like2 (D-glucose-2-phosphate-2-glucose, an analogue of agrocinopine D, see the Methods section) as the sole carbon source. Under these conditions, Bo542 cells did not grow on L-arabinose-2-phosphate and agrocinopine A, in contrast to C58 cells. Therefore, these results showed that AccABo542 associated to its ABC transporter cannot assimilate opines containing the arabinose-2-phosphate moiety (Figures 2A-E).

In order to exclude that factors located on the chromosome or other plasmids than the pTi might influence agrocinopine (or derivative) assimilation, we also conducted growth assays comparing four different strains: C58 (containing pTiC58), C58 lacking the pTi (referred to as C103), C58 devoid of both pTi and pAt (referred to as C58:00), and C58pTiBo542 (cured of pTiC58 and containing pTiBo542, referred to as LBA288 (23)). As expected, the strain C58:00, which possesses only the chromosomal elements, displayed no growth on D-glucose-2-phosphate, in contrast to both C58 and LBA288, which carry a pTi plasmid (Figure 2F). Furthermore, the absence of growth for the strain C103 on D-glucose-2-phosphate confirmed that the pAt plasmid has no effect on the agrocinopine (or

derivative) uptake process. Similarly to Bo542, LBA288 (C58pTiBo542) did not grow on A2P and agrocinopine A.

In previous studies, we showed that *A. fabrum* strain C58, upon uptake of agrocinopine A, L-arabinose-2-phosphate or D-glucose-2-phosphate, initiates the production of the quorum-sensing (QS) signal, leading to the synthesis of 3-oxo-octanoylhomoserine lactone (OC8HSL). This, in turn, induces the amplification of copy number and facilitates the conjugation of the pTi (10). In both Bo542 and C58 strains, opines/analogues containing the D-glucose-2-phosphate moiety can activate the synthesis of OC8HSL and promote pTi conjugation (Figure 3), in agreement with their observed uptake patterns (Figure 2).

Strain containing pTiC58 has a competition advantage over the strains harboring pTiBo542 on D-glucose-2-phosphate uptake. Competitions between C58 and Bo542 or LBA288 (C58pTiBo542) strains at a 1:1 ratio were performed in both rich medium and in AB medium supplemented with D-glucose-2-phosphate as sole carbon source. After 36 h of culture in the rich medium, the bacterial level remained similar. In contrast, in the presence of D-glucose-2-phosphate (G2P), a noticeable fitness advantage was observed for the C58 strain, reaching 80% and 90% prevalence in competitions with Bo542 and LBA288, respectively. This implies that D-glucose-2-phosphate was more efficiently assimilated by the strain containing pTiC58 compared to the strains harboring pTiBo542 (Figure 4).

AccABo542 is more stable than AccAC58 and exhibits lower affinity for D-glucose-2-phosphate and agrocinopine D-like2 than AccAC58. Analyses of thermal denaturation experiments by DSC showed a different profiles distribution between AccABo542 and AccAC58. Apo AccAC58 (T*m* of 57.27°C) displays a lower T*m* by 6.55°C compared with AccABo542 (T*m* of 63.82°C) meaning that AccABo542 is more stable (Figure S2, Table 1A). Addition of D-glucose-2-phosphate or a compound containing the arabinose-2-phosphate moiety (L-arabinose-2-phosphate or agrocinopine A) did not alter the T*m* of AccABo542 whereas addition of agrocinopine D-like2 slightly increased it by ~2.83°C. Unlike AccABo542, each of the four compounds tested induced large shifts of T*m* for AccAC58. The largest of 7.16°C and 9.33°C were observed with the D-glucose-2-phosphate and agrocinopine D-like2, respectively (Figure S2). The binding of agrocinopine A and its short derivative to AccAC58 resulted in a lower T*m* compared to apoAccABo542.
The same approach by nano-differential scanning fluorimetry (nanoDSF) on a Tycho NT.6 instrument led to a similar analysis of results as DSC although the T*i* shifts were more pronounced (Figure S3, Table 1B).
Binding of ligands to AccABo542 and AccAC58 was further explored using tryptophan fluorescence spectroscopy (AccABo542 and AccAC58 possess 11 and 12 tryptophans, respectively) and isothermal titration microcalorimetry (Figure S4, Table 2). No interaction could be measured between AccABo542 and L-arabinose-2-phosphate or agrocinopine A using both approaches. Intrinsic protein fluorescence titration experiments for AccABo542 yielded apparent dissociation constant K_D values of 15 µM and 1.6 µM with D-glucose-2-phosphate and agrocinopine D-like2, respectively. AccAC58 displayed higher affinity for both ligands by at least 12 fold compared with AccABo542. For both proteins, affinity was about 10-fold higher for agrocinopine D-like2 than for D-glucose-2-phosphate.
Using isothermal titration microcalorimetry, the binding of D-glucose-2-phosphate and agrocinopine D-like2 to AccABo542 showed similar K_D values compared to autofluorescence. For AccAC58, slightly higher affinities were determined. Microcalorimetry data confirmed the 1:1 binding stoichiometry revealing a similar negative enthalpy change for each AccA suggesting similar protein-ligand interactions.

Structural study of AccABo542. Apo AccABo542 crystallized in two different space groups, with different packing for each space group and one or two molecules in the asymmetric unit (PDB 8C6W, 8C6Y, 8C75 and 8C6R in Table 3). The four different crystal forms, namely Forms 1 to 4 led to six very similar AccABo542 molecules as indicated by the average root mean square deviation (RMSD) of 0.52 Å for all Cα atoms. The monomeric AccABo542 possesses a typical fold of cluster C within the SBP structural classification (24) (Figure 5A). The N-terminal lobe (the biggest named lobe1) consists of residues (31-280 and 495-521) and the C-terminal lobe (lobe 2) comprises residues 284-491. Two short segments define the hinge region connecting the two lobes. All apo AccABo542 and apo AccAC58 (PDB 4ZE8) are similar, displaying a RMSD of 0.67 Å for 490 Cα atoms between Form 3 (PDB 8C75) and 4ZE8 (Figure 5B). Co-crystallization of AccABo542 with D-glucose-2-phosphate (G2P) was unsuccessful. The liganded structure was obtained by soaking the unliganded Form 3 crystals with G2P, resulting in the change of the space group $P2_1$ to $P2_12_12_1$ (PDB 8CB9, Table 4) due to the lobes closure upon ligand binding. Indeed, when lobes 1 of the unliganded and G2P structures are superimposed (overall RMSD of 1.71 Å for 474 Cα atoms), we observe a 9° rotation around the hinge residue Tyr493 allowing lobe 2 to move towards lobe 1 for ligand trapping (Figure 5C). Five residues (134-138) are not visible in the electron density maps. The co-crystal structure of AccABo542-agrocinopine D-like2 (AgroD-like2, PDB 8CAY) also in the closed conformation is similar to AccABo542-G2P structure with a RMSD of 0.95 Å for all Cα atoms.
The common glucose-2-phosphate moiety of G2P and AgroD-like2 is fully defined in the electron density maps and bound at the same position between the two closed lobes of AccABo542 making identical protein contacts up to 3.4 Å (Figures 5D and 5E). The OH1 group of the glucose adopts two anomeric forms in all ligands, either α or β at 50% each. The β anomer is anchored by 4 hydrogen bonds involving the side chains of Asn54 and Glu510 from lobe 1, Asn284 from the hinge region and Ser419 from lobe 2, whereas the α anomer interacts with Glu510 only (Figure 5D and Figure S5). In the rest of the text, we will focus on the β anomer of the glucose motif for the structural comparison between AccABo542 and AccAC58 because of its additional protein contacts compared with the alpha anomer. The OH3, OH4, OH6 and OH5 groups interact with the side chains of Trp418, Glu434, Glu434 and the main chain NH of Gly421, respectively. In addition to their glucose interactions, Asn54 and Ser419 with the help of Tyr375 and Tyr376 hold the phosphate oxygens. In contrast, the second glucose of AgroD-like2 makes only one protein contact with the carbonyl group of Ile52 and a hydrogen bond is formed between both OH3 of each glucose (Figure 5E). All attempts to co-crystallize or soak unliganded AccABo542 crystals with ligands containing an arabinose-2-phosphate moiety were unsuccessful.

Structures comparison between AccAC58 and AccABo542. We previously reported the structures of the mature AccAC58 in complex with agrocinopine A (AgroA, PDB 4ZEB) and different derivatives including L-arabinose-2-phosphate (PDB 4ZEI) and D-glucose-2-phosphate (PDB 4RA1) (10). When we were trying to co-crystallize AccABo542 in excess of AgroA, we co-crystallized AccAC58 and AgroA in parallel as a control. In this study, we obtained a 1.29 Å resolution structure of AccAC58-AgroA in a new space group (I222, PDB 8CKE (Table S1) versus C2, PDB 4ZEB at 1.9 Å resolution (10)). This higher resolution structure highlighted the presence of two anomers for the OH1 of the arabinose, as observed for the glucose within the pyranose-2-phosphate motif, and allowed us to correct the conformation of the last glucose of the sucrose moiety of AgroA (Figure S6A). Nonetheless, this structure resembles the previous one (0.44 Å RMSD for all Cα atoms and a 2° rotation difference in domain closure). The numerous interactions previously described (10) between

AccAC58 and AgroA are confirmed. Most of these interactions (12 hydrogen bonds) occur between the arabinose-2-phosphate moiety and AccAC58 whereas only four are observed between the sucrose moiety of AgroA and the protein (Figure S6B).
Crystals of AccAC58-AgroD-like2 complex (PDB 8CKD, Table S1) which diffracted to 1.6 Å resolution are isomorphous to AccAC58-AgroA crystals (PDB 8CKE). Both complexed structures are nearly identical as shown by a RMSD of 0.19 Å for all Cα atoms meaning that the domain closure is the same. Similarly to AgroA, most of the protein interactions involve the pyranose-2-phosphate motif of AgroD-like2 (Figure 5F). Superposition on 490 Cα atoms of AccABo542 and AccAC58 in complex with either G2P (PDB 8CB9 and 4RA1) or AgroD-like2 (PDB 8CAY and 8CKD) gives a RMSD of 0.81 and 0.78 Å, respectively, indicating a similar fold and domain closure. Moreover, the ligands occupy the same position in the ligand binding site of AccABo542 and AccAC58 (identical for the G2P moiety), making very similar interactions with the proteins due to highly conserved amino-acids in the ligand pocket (Figures 5D-I). The unique and major difference concerns the amino acid Phe145 (Tyr 145 in AccAC58), which is responsible for the loss of one hydrogen bond for the G2P moiety in AccABo542 compared to AccAC58 (Figures 5H and 5I).

***A. vitis* strain S4 is insensitive to the antibiotic agrocin 84 since it possesses a silent *acc* operon**. When conducting a search for agrobacteria pathogenic strains featuring an Acc transport system and displaying resistance to the antibiotic agrocin 84, which can eliminate the strains C58 and Bo542 through its TM84 component, we came across *Agrobacterium vitis* strain S4 based on literature.
We first performed a structural and biochemical study of AccAS4 protein, aiming at finding out an AccA protein specific to arabinose-2-phosphate (A2P) and AgroA. Unfortunately, DSC, nanoDSF and autofluorescence showed that AccAS4 was able to bind all agrocinopines and derivatives, similarly to AccAC58 (Figure S7). Apo AccAS4 presented the lowest T*i* of 51°C compared to 63.1°C and 69.7°C for AccAC58 and AccABo542, respectively. Ligand binding shifted the T*i* to 57.3°- 62.9° showing therefore a significant increase of ~6-12°C. The same approach by nanoDSF led to similar results as DSC. Using tryptophan fluorescence spectroscopy, titration experiments yielded apparent K_D values of 1.01 µM, 1.17 µM, 0.3 µM and 1.21 µM for AgroA, A2P, AgroD-like2 and G2P, respectively (Figure S7), which are comparable to those previously measured for AccAC58 (10) and presently described in Table 2.
The high-resolution structures of AccAS4 in complex with A2P, G2P, AgroA, AgroD-like2 or agrocin 84 were solved in the same space group with one molecule in the asymmetric unit. Each ligand is very well defined in electron density maps for the pyranose-2-phosphate-like motif and AgroA is completely modeled, in contrast to the TM84 moiety of agrocin 84 (Table S2, Figure S8). A2P, G2P and AgroA displayed two anomers for their OH1 group on the pyranose-2-phosphate motif whereas AgroD-like2 and agrocin 84 showed an alpha anomer. All liganded structures are very similar to each other (average RMSD of 0.27 Å for all Cα atoms) and share a domain closure similar to both liganded AccAC58 and AccABo542 (0.99 Å average RMSD between 466 and 490 Cα atoms). Most of the ligand-protein interactions occur *via* the pyranose-2-phosphate-like motif as observed for AccAC58 and AccABo542. The pyranose-2-phosphate-like motifs superpose well with both liganded AccABo542 and AccAC58, unlike the TM84 part of agrocin 84 (PDB 8CAW for AccABo542, this study and PDB 4ZEC for AccAC58 (10) even if its phosphate group is held by the conserved arginine 444 (Figure 6).
Although AccAS4 can bind A2P, G2P, AgroA and AgroD-like2, the strain S4 cannot grow using any of these compounds as a nutrient source (Figure S9A). Similarly, even if AccAS4 can interact with agrocin 84, the strain S4 remains insensitive to the toxic TM84 moiety. We then investigated the lack of import by evaluating the *acc* operon gene expression using a transcriptional reporter fusion between

the C58 or S4 *acc* promoter and *egfp* gene, introduced in each strain. As expected, compared with the fluorescence level measured in AB medium without inducer, the fluorescence level measured in the presence of A2P was significantly higher for the P*acc*C58 reporter fusion in the strain C58 (e.g. *acc* operon promoter from C58 cloned in the reporter plasmid pOT1e and introduced in the strain C58). For P*acc*S4 introduced in the strain C58, we did not observe A2P-induced fluorescence. When the same experiments were performed using the strain S4, A2P had an inductive effect for P*acc*C58 only whereas P*acc*S4 reporter fusions was not induced, therefore suggesting that P*acc*S4 was not recognized by any transcription factor (Figure S9B).

L-arabinose-2-phosphate could be modeled in AccABo542 binding site. Superimposing the structures of AccAC58 or AccAS4 in complex with A2P (PDB 4ZEI and 8CH2, respectively) on AccABo542-G2P complex (PDB 8CB9), we observed that A2P and G2P overlapped (Figure 7A). It was then straightforward to place a bound A2P manually to AccABo542 instead of G2P, revealing that the interactions between A2P and AccABo542 are very similar to those between A2P and AccAC58/AccAS4 (Figures 7B-D). Indeed, the 10 amino-acids Asn54, Asp284, Tyr375, Tyr376, Trp418, Ser419, Asn420, Gly421, Glu434 and Glu510 in direct interaction with the arabinose-2-phosphate moiety of agrocinopines A/B are strictly conserved as shown in the structure-based sequence alignment (Figure 8).
AccABo542, AccAC58 and AccAS4 share 19 residues (red triangles in Figure 8) out of the 25 amino acids defining the ligand binding site and binding the ligand *via* polar or hydrophobic contacts, namely residues Ile52, Ser53, Asn54, Trp178, Asn284, Met372, Tyr375, Tyr376, Arg416, Trp418, Ser419, Asn420, Gly421, Trp423, Thr430, Glu434, Arg444, Trp445 and Glu510. Out of the six remaining residues, Thr/Ser/Gly406 and Thr/Phe/Ala407 (orange triangles in Figure 8) are not conserved and the other four (green triangles in Figure 8) differ in AccABo542 compared to AccAC58/AccAS4: Asn141, Phe145, Phe402 and Gly440 in AccABo542 correspond to Leu141, Tyr145, Tyr402 and Gln440 in AccAC58/AccAS4. Among them, Tyr145 is the sole residue interacting with the glucose-2-phosphate moiety of agrocinopines C/D and agrocin 84 in AccAC58 and AccAS4 and Gln440 the sole to bind the sucrose moiety of agrocinopine C-like as observed in AccAS4 (Figures 5F-G, S8C-D and 6C).
We thus mutated these two amino acids Phe145 to Tyr145 and Gly440 to Gln440 to make AccABo542 resemble AccAC58 and AccAS4 for the binding pocket. The structure of the apo double mutant AccABo542F145YG440Q solved at 1.84 Å resolution (PDB 8C6U, Table 3) confirmed the presence of both mutations and superposes to the apo wild-type structure with an average RMSD of 0.56 Å for all Cα atoms (Figure S10A). Both mutations slightly increased the stability of AccABo542F145YG440Q compared to the wild-type protein. In agreement, G2P and AgroD-like2 binding had a modest effect on the protein mutant stability measured by DSC and a slightly higher effect measured by nanoDSF as observed for the wild-type AccABo542 (Figures S3, S4 and S10B-C). Nonetheless, this was not comparable to the drastic effect of ligand binding on AccAC58 and AccAS4 stability. AccABo double mutant cannot bind A2P and AgroA as observed for the wild-type protein. No interaction could be measured between AccABo542F145YG440Q and L-arabinose-2-phosphate or agrocinopine A using tryptophan fluorescence spectroscopy and isothermal titration microcalorimetry. Affinity measured by autofluorescence of the double mutant towards G2P was 3-fold higher compared with the wild-type protein (Figure S10D), however not as high as measured for AccAC58, meaning that these mutations are not sufficient to make AccABo542 similar to AccAC58 for the ligand binding.

AccAC58, AccABo542F145YG440Q and AccAS4 show different selectivity towards the synthesized agrocinopine-C-like2. We co-crystallized AccAC58 wild-type, AccAS4 wild-type, and

the double mutant AccABo542F145YG440Q with the freshly synthesized agrocinopine C-like2 (Tables S1, S2 and 4). The high-resolution electron density maps of each structure revealed a different bound ligand and none was an AgroC-like2 compound (Figures S1 and 9). All were a D-glucose-2-phosphate linked to sucrose either via the glucose first (observed in AccAC58 with AgroC-like3, PDB 8CKO and AccAS4 with AgroC-like4, PDB 8CH3) or the fructose first (observed in AccABo542F145YG440Q with AgroC-like1', PDB 8CDO). The agroC-like2 solution was thus composed of a mixture of isomers and each AccA selected a different isomer. The common glucose-2-phosphate moieties bind similarly and superpose very well upon structural comparison, unlike the sucrose part (Figure 9D). Nonetheless, the localization of the sucrose part in both AgroC-like1' (in AccABo542F145YG440Q) and AgroC-like3 (in AccAC58), composed of a fructose-glucose and a glucose-fructose, respectively, is similar inside the ligand binding site (Figure 9D). A slight movement of the loop 402-407 can accommodate the sucrose moiety. It is noteworthy that both fructoses ending AgroC-like3 and AgroC-like4 are not well defined in the electron density maps in contrast to the fully defined AgroC-like1' bound to the AccABo542 mutant. Superposition of AccAC58 and AccAS4 in complex with AgroA showed full overlapped AgroA unlike AgroC-like, for which a different linkage between the phosphate and the sucrose results in an opposite position of the last fructose in the ligand binding site (Figure 9).

Domain dynamics of AccABo542 and AccAC58 are different. The global dynamics between the apo crystal forms of AccABo542 (PDB 8C75) and AccAC58 (PDB 4ZE8) are dramatically different as shown by the RMSD along the molecular dynamics (Figures 10 and S11). Globally, AccABo542 appears remarkably stable compared to AccAC58. Based on the RMSF comparison of each residue between the apo forms, we identified the dynamic differences in five regions: two regions in lobe 1 with residues 48-60 (box n°1) and 89-103 (box n°2) highlighted in blue and green boxes, respectively and three regions of lobe 2, which are residues 325-352 (box n°3), 414-445 (box n°4) and 450-483 (box n°5) shown in red, orange and purple boxes, respectively (Figures 10A). Interestingly, the two most flexible regions n°3 and 5 shown in red and purple, respectively are not involved in the formation of the binding site in contrast to the blue (n°1) and orange (n°4) regions (Figures 10D-E). In the closed form of AccAC58 (PDB 8CKD where we removed the ligand), the regions n°2, 4 and 5 became very stable, and the region n°3 was drastically less flexible (Figure 10B). Remarkably, the closed form of AccABo542 (PDB 8CAY with the ligand removed) has the flattest RMSF profile and the dynamics between the apo and closed forms of AccABo542 are quite similar (Figure 10C), in agreement with the results from DSC and Tycho revealing weak shifts of T*m* and T*i* upon ligand binding. As expected, the global dynamics between both empty closed forms of AccABo542 and AccAC58 indicated very few differences compared to both apo forms (Figure S11).

Discussion

The T-DNA part of the pTi of the pathogenic *Agrobacterium* strains C58 and Bo542 encodes genes able to synthesize agrocinopines A/B and C/D respectively, once integrated into the plant genome. The remaining part of the pTi harbors the *acc* operon, responsible for agrocinopine import via the SBP AccA-ABC transporter and degradation *via* the enzyme AccF of the opine agrocinopine. We previously demonstrated that the SBP AccAC58 can bind all agrocinopines by means of a common sugar key-recognition motif (a pyranose-2-phosphate motif), which is L-arabinose-2-phosphate (A2P) or D-glucose-2-phosphate (G2P) in agrocinopines A/B and C/D, respectively (10). Therefore, the strain C58 which was originally defined as specific for the agrocinopines A and B can also assimilate the opine agrocinopines C and D, which are produced during the plant infection by the strain Bo542. Here, we showed that the strain Bo542 can only assimilate its own agrocinopines C and D and

derivatives containing a D-glucose-2-phosphate moiety meaning that AccABo542 displays a different specificity compared to AccAC58. We validated that, for both Bo542 and C58 strains, the G2P motif resulting from agrocinopine C/D cleavage due to AccF enzyme is active by binding to the transcriptional repressor AccR. G2P-AccR complex relieves repression, leading to formation of many products including Acc proteins and the transcriptional activator TraR. TraR by interacting with the quorum-sensing (QS) molecules (OC8HSL produced by TraI) stimulates the expression of the QS-regulated genes, including *traI* and activates the dissemination of the pTi by horizontal transfer (by bacterial conjugation) as observed for both strains C58 and Bo542 (25).

Similarly to C58, strain Bo542 is sensitive to the antibiotic agrocin 84, which possesses a D-glucose-2-phosphoramidate moiety, resembling the G2P motif. Indeed, both C58 and Bo542 Acc transport system import the antibiotic agrocin 84. In contrast, we confirmed that the *A. vitis* strain S4 responsible for the crown gall disease of grapevine is insensitive to agrocin 84 (26) although it harbors an *acc* operon, highly similar to that of the strain C58 and with the same gene organization. Indeed, a gene homologous to *accR* (76% sequence identity) is present upstream S4 *accA* gene. Unexpectedly, we found that the *acc* operon S4 is located on the chromosome 1 and not on the pTi. We confirmed this unexpected localization by the transfer of the pTi from the strain S4 into a bacterial strain devoid of pTi. We observed the absence of *accA* gene in the resulting transformed bacteria (data not shown). Moreover, we showed that this operon is never transcribed in the presence of inducers such as A2P or G2P in both the strains S4 and transformed C58 strains. Therefore, the insensitivity to agrocin 84 is explained by the lack of expression of the Acc transport system making agrocin 84 import impossible. This is in line with our data showing that the strain S4 cannot grow using agrocinopines or derivatives as a nutrient source. Altogether, these findings suggest that the presence of the *acc* operon on the S4 chromosome is probably linked to horizontal gene transfer and has no real function so far. This confirms that the pTi of the strain S4 is devoid of *acc* operon, in line with the observation that its T-DNA part synthesizes at least two opines (vitopine and rideopine) in plants and not agrocinopines (27).

When we started this work a few years ago, we synthesized agrocinopines C and D based on their reported structure and previously published synthesis, consisting of D-glucose-2-phosphate-2-glucose-fructose (AgroC-like2) and of D-glucose-2-phosphate-2-glucose (AgroD-like2), respectively (Figures 1 and S1) (28). Nonetheless, the very recent NMR structure of the natural agrocinopine C revealed a G2P linked in a phosphodiester bond to the sixth carbon of the glucose moiety of a sucrose molecule (D-glucose-2-phosphate-6-glucose-1-2-fructose, Figure 1) (29). Therefore, although our synthetic agrocinopines C and D appeared to be incorrect, they turned out to be analogues of agrocinopines C/D useful for this study. Indeed, they did not alter our work because so far, the SBP AccA recognizes either A2P and G2P moieties or G2P moiety only, which is the functional part of agrocinopines in bacteria. High resolution electron density maps revealed that AgroC-like2 was a mixture composition of G2P linked to sucrose either via the glucose first or the fructose first. Such by-products can arise from migrations of acetyl groups in intermediate 1 when placed under basic conditions for the coupling with phosphoramidate 2. Indeed, OH-2 is known to be quite nucleophilic, and able to react with the neighboring 3-O-acyl group, leading to the hepta acetyl sucrose with only OH-3 unprotected. Further migrations to O4 can also occur (Figure S1). Reaction of OH2 with the 1'-O-acyl group of the fructose is also possible, since the required intermediate 8-membered ring 2-1' for such a migration is actually observed in sucrose chemistry (30). Migrations of the phosphate ester cannot be ruled out either, notably during the deprotection scheme after the deactylation step, with OH-3 or OH-1' ready to undergo transphophatations on the 2-phosphodiester. Interestingly, AccABo542, AccAC58 and

AccAS4 selected different isomers namely agroC-like1', agroC-like3 and agroC-like4, respectively, from the same mixture of synthetic AgroC-like2 (Figure S1), despite sequence identity between 75 and 91% and a nearly identical ligand binding site. Their common G2P moiety makes numerous protein interactions unlike their different sucrose part (Tables 4, S1-2). This suggests that the specificity is more complex than just the mere selection of the common G2P moiety. Ligand preference seems to occur beyond the G2P motif recognition, likely due to ligand plasticity to accommodate the ligand binding site. Of particular note is that AgroD-like2 has a better affinity than G2P for each AccA meaning that the ligand length has also an effect on selectivity.

Understanding the specific determinants of protein specificity requires detailed experimental investigations and structural analysis. In the case of AccA, we obtained numerous structures, which unfortunately did not bring insight. The most striking result was the absence of any steric hindrance and/or any crucial interaction loss in the ligand binding site of AccABo542, preventing the binding of A2P in silico. All amino-acids residues that interact directly with A2P are conserved among the three AccA arising the issue of why AccABo542 cannot bind agrocinopines A/B *in vitro* and *in vivo*. Moreover, mutating two amino acids (F145Y and G440Q) in the vicinity of the ligand pocket of AccABo542 to make it resemble that of AccAC58 did not modify the protein selectivity and stability and did not enhance ligand affinity, emphasizing that AccABo542 specificity was not due to the first shell of amino-acids surrounding the ligand. An outcome of this work was the remarkable difference in stability between the SBPs AccABo542, AccAC58 and AccAS4 despite high sequence identity. Because apo AccBo542 is far more stable than AccAS4 and AccAC58, it crystallizes easily. To our knowledge, AccaBo542 is the first example of SBP for which many different crystals of apoform were obtained. SBPs are subject to conformational changes induced by ligand binding and present diversity in conformational and dynamic plasticity (31). In agreement, crystallization of apo AccAS4 was unsuccessful despite several attempts, and getting a crystal of apo AccAC58 was a long-term effort (10). In contrast, as shown by molecular dynamics simulation and DSC on both liganded AccAC58 and AccABo542, once liganded, SBPs are in a closed state and highly stable to bring the ligand to their ABC transporter. Molecular dynamics on apo AccAC58 revealed a few highly flexible regions located outside the ligand binding site. This higher flexibility and conformational dynamics of AccAC58 seem to contribute to its broader selectivity and thus its ability to interact with any agrocinopines/derivatives, moreover, this with higher affinity than AccABo542. Conversely, AccABo542, which is more stable and thus more rigid has a narrower range of conformational space available to accept and accommodate ligands, making AccABo542 specific for agrocinopines C/D. The interplay between chemical properties of the ligands, protein plasticity, dynamics, stability and other determinants such as steric complementarity or/and protein-ligand interactions, in determining specificity is a complex area of research.

Methods

Synthesis of agrocinopines and derivatives. Agrocinopine A and agrocin 84 used in this study were the same used as in our first published work on AccAC58 (10). L-arabinose-2-phosphate (A2P) and D-glucose-2-phosphate (G2P) were freshly prepared as described (10). Regarding agrocinopines C and D, the synthesis was based on their reported structure and previously published synthesis at the time we started this work, consisting of D-glucose-2-phosphate-2-glucose-fructose and of D-glucose-2-phosphate-2-glucose, referred below as AgroC-like2 and AgroD-like2, respectively (Figures 1 et S1) (28). Nonetheless, the latter appeared to be incorrect as proved by the very recent NMR structure of the natural agrocinopine C, which is a D-glucose-2-phosphate linked in a phosphodiester bond to the sixth carbon of the glucose moiety of a sucrose molecule (D-glucose-2-phosphate-6-glucose-1-2-fructose, Figure 1A) (29). The synthesis of agrocinopine C-like2 was achieved as shown in the scheme of Figure S1A from the 1',3,3',4,4',6,6'-hepta-*O*-acetyl sucrose **1** prepared according to (32). Condensation of this latter with the intermediate glucoside **2** (10) bearing a phosphoramidate group at O2 in the presence of tetrazole as the base followed by oxidation led to the fully protected AgroC-like2 **3**. Removal of all ester groups was achieved first by basic treatment with sodium methoxide before palladium catalyzed hydrogenolysis of benzyl groups led to the targeted compound AgroC-like2. Using mass spectrometry (Figure S1B) and comparison with reported NMR data, the synthesized AgroC-like2 was at the expected molecular mass and rather pure. Nonetheless, our structural study revealed that AgroC-like2 was a mixture composition of D-glucose-2-phosphate linked to sucrose either via the glucose first or the fructose first. Other isomers are fully consistent with the presence of namely AgroC-like1', AgroC-like3 and AgroC-like4 (Figure S1A). Agrocinopine D-like2 was prepared as reported in our earlier work (21). In the structural part of the manuscript, we will use the short names of agrocinopines and analogues such as G2P, AgroD-like2, AgroC-like2, AgroC-like1', AgroC-like3, AgroC-like4, A2P and AgroA.

Bacterial culture conditions. Strains of *A. fabrum* C58 (containing pTiC58), LBA288 (C58pTiBo542, generously provided by P. Hooykaas (23)) and derivatives (C103 (C58 lacking the pTi plasmid) and C58:00 (cured of pTi and pAt)), *A. tumefaciens* Bo542 (containing pTiBo542) and *A. vitis* S4 were cultivated overnight at 28°C in AB medium supplemented with succinate. Overnight cells were washed with 0.8% NaCl and transfered in 200 µl of AB medium supplemented with 2 mM of carbon sources (succinate, agrocinopine A, agrocinopine D-like2, L-arabinose-2-phosphate or D-glucose-2-phosphate). OD_{600nm} representing the cells growth in 96-well microplates was measured every 20 min during two days using Tecan Infinite 200 R (Tecan, Männedorf, Switzerland). Analyses were performed in four technical replicates and in two biological replicates.

Competitions assays between the strains Bo542 or LBA288 (C58pTiBo542) and C58. Competition for carbon sources were determined using a kanamycin-resistant derivative of *A. fabrum* C58 (pTi*atu6148*:Km) and *A. tumefaciens* Bo542 or LBA288 (C58pTiBo542 (23)), as previously described (33). After growth in yeast peptone glucose (YPG)-rich medium, overnight cells were washed with 0.8% NaCl and the optical density at 600 nm was adjusted at 1. Strains were mixed in equal volume (1:1 ratio), and 10 µl of the mixture was used to inoculate 200 µl of YPG medium or AB supplemented with 2 mM of D-glucose-2-phosphate as carbon source. The input ratio of the initial inoculum was determined by plating the initial inoculum onto YPG agar medium or YGP agar medium containing kanamycin and neomycin (each at 25 µg/ml) to determine the relative proportions of the two strains. After 36 h of growth at 28°C with agitation, the output ratio was determined on the same medium. Two independent assays were conducted, each with five technical replicates. The proportions of C58 and Bo542 or LBA288 strains between the initial strain ratio and the output ratio in

YPG or AB supplemented with D-glucose-2-phosphate media were compared using a student test (p-value = 0.05), performed with the R software.

Conjugation assays and quantification of OC8HSL. Overnight LBm cultures of recipient (C58.00, a strain devoid of pTi) and donor (Bo542) cells were mixed in an equal ratio (1:1). 10 µl of this mix were transferred into 140 µl of AB medium supplemented with mock or 1 mM of inducer (L-arabinose-2-phosphate, D-glucose-2-phosphate, agrocinopine A and agrocinopine D-like2) for liquid cultures of 24, 48, 72 and 96 hours. Suspension dilutions of these cultures were spotted onto selective agar media to enumerate the different bacterial populations (donor, recipient and Ti plasmid transconjugants). In parallel, to quantify OC8HSL, aliquots of cell cultures were spotted onto TLC plates (RP-18/UV254, Macherey-Nagel) and incubated 48 h at 28°C in an AB mannitol medium with the OC8HSL-bioindicator *A. tumefaciens* strain NT1(pZLR4) as previously described (34) (10). Tested samples were compared with a calibration curve obtained with pure OC8HSL (Sigma-Aldrich).

Cloning, expression and purification of AccA proteins from the strains of *A. fabrum* C58, *A. tumefaciens* Bo542 and *A. vitis* S4. The sequence corresponding to the mature AccAC58, AccABo542 and AccAF145YG440QBo542 expression plasmids were obtained by chemical synthesis of the corresponding *accA* gene without the signal sequence of 29 and 30 amino acids for AccA58 and AccABo542, respectively, that serves for the localization to the bacterial periplasm. A C-terminal hexahistidine tag was added into the plasmid pET9a (Genscript, NJ, USA). The mature AccAS4 without the signal sequence of 29 amino acids and containing a C-terminal hexahistidine tag was amplified by PCR using the following primers: surexAccAS4F (CCCTCTAGAAATAATTTTGTTTAACTTTAAGAAGGAGATATACATATGGCCGAGCGCCGC) and surexAccAS4R (GCACTCGAGGCCGAAAGCAAGGTTGTTGC). The PCR product was ligated into the plasmid pET20b digested with XbaI-XhoI enzymes. The recombinant plasmid was transformed into *E. coli* BL21 pLysS. Each AccA protein was expressed and purified as previously described (10).

Differential scanning calorimetry (DSC). Thermal stability of each AccA and each complex was performed by DSC on a MicroCal model auto PEAQ DSC (Malvern) in a standard buffer with 5 µM and 50 µM for protein and ligand, respectively. Each measurement was preceded by a baseline scan with the standard buffer. All solutions were degassed just before loading into the calorimeter. Scans were performed at 1 $K.min^{-1}$ between 20 and 90°C. The heat capacity of the buffer was subtracted from that of the protein sample before analysis. Thermodynamic parameters were determined by fitting the data to the following equation:

$$\Delta C_p(T) = \frac{K_d(T)\,\Delta H_{cal}\,\Delta H_{vH}}{[1 + K_d(T)]^2\,RT^2}$$

where *K*d is the equilibrium constant for a two-state process, Δ*H*vh is the enthalpy calculated on the basis of a two-state process and Δ*H*cal is the measured enthalpy.

Tycho NT.6 Nanotemper Differential Scanning Fluorimeter. This equipment measures the change in intrinsic fluorescence of tryptophan residues in protein samples (20 µM and 200 µM for protein and ligand, respectively). Protein unfolding was followed by tryptophan fluorescence intensity at 330 and 350 nm in the presence of different ligands (same as for DSC). The inflection temperature (T_i) was determined by detecting the maximum of the first derivative of the fluorescence ratios (F_{350}/F_{330}) after

fitting experimental data with a polynomial function. Data were measured in triplicate. Tycho NT.6 was used with a heating rate of 30°C min^{-1}.

Fluorescence titration measurements. Each ligand bound to each AccA was monitored by autofluorescence by excitating the protein at a wavelength of 295 nm and monitoring the quenching of fluorescence emission of tryptophans at 335 nm. All experiments were performed at 20°C in 96 well plates (1/2 Area Plate-96F, Perkin Elmer) using Tecan Infinite M1000 (Tecan, Männedorf, Switzerland) in 50 mM Tris-HCl pH 8.0 and 150 mM NaCl with a fixed amount of proteins (2 and 5 µM) and increasing concentrations of ligand. Each ligand has no emission signal at 335 nm. The data were analyzed using Origin® 7 software and fitted to the equation $f=\Delta Fluorescence_{max}*abs(x)/(K_D+abs(x))$.

Isothermal titration microcalorimetry measurements. Isothermal titration microcalorimetry experiments were performed with an ITC200 or a PEAQ ITC isothermal titration calorimeter from MicroCal (Malvern Panalytical, Malvern, UK). The experiments were carried out at 20°C with a protein concentration of 50 µM. 19 injections of 2 µl of ligand solution at a concentration of 600 µM were performed at intervals of 180 s while stirring at 500 rpm. The experimental data were fitted to theoretical titration curves with software supplied by MicroCal (ORIGIN® Northamption, MA, USA). This software uses the relationship between the heat generated by each injection and ΔH (enthalpy change in $Kcal.Mol^{-1}$), Ka (the association binding constant in M^{-1}), n (the number of binding sites), total protein concentration and free and total ligand concentration (35).

Crystallization of AccA and structure determination. AccAC58 was co-crystallized with agrocinopine A, agrocinopine D-like2 and agrocinopine C-like2 but agrocinopine C-like3 was present in the structure, as previously described according to the condition B (20% PEG 4000, 200 mM ammonium acetate and 100 mM sodium citrate pH 5.6 (10) Table S1. Crystallization conditions for apo AccABo542 and apo AccAF145YG440QBo542 at 25 mg/mL were screened using Qiagen kits (Valencia, CA, USA) with a Mosquito (SPT Labtech, Melbourn, UK). The crystals were manually reproduced in hanging drops experiments by mixing equal volumes of protein solution and precipitant solution mentioned in Table 3. Crystallization conditions for AccABo542 at 40 mg/mL in the presence of 1.5-2 mM ligands (L-arabinose-2-phosphate, agrocinopine A, D-glucose-2-phosphate, agrocinopine D-like2, agrocin 84) and for AccAF145YG440QBo542 (agrocinopine C-like2 but agrocinopine C-like1' was present in the structure) were screened and crystals were manually reproduced (Table 4). Our trials to co-crystallize AccABo542 with L-arabinose-2-phosphate, agrocinopine A and D-glucose-2-phosphate were unsuccessful. By soaking the apo Form3 with 10 mM D-glucose-2-phosphate, we obtained a liganded structure. Crystallization conditions for AccAS4 at 16 mg/mL in the presence of 2 mM ligands (agrocinopine A, L-arabinose-2-phosphate, agrocinopine D-like2, D-glucose-2-phosphate, agrocinopine C-like2 but agrocinopine C-like4 was present in the structure and agrocin 84) were also screened and crystals were manually reproduced (Table S2). All crystals were transferred to a cryo-protectant solution (mother liquor supplemented with 25% PEG 400) and flash-frozen in liquid nitrogen. All diffraction data were collected at 100 K on the PROXIMA 1 and 2 beamlines at synchrotron SOLEIL (Saint-Aubin, France). Diffraction intensities were integrated by the XDS program (36) using either xdsme (github.com/legrandp/xdsme) or autoPROC (www.globalphasing.com) including STARANISO (37). The crystal structures were all determined by molecular replacement with PHASER (38) using the AccAC58 models (PDB codes 4ZEB or 4RA1) as search models or the new models obtained in this study. Refinement of each structure was performed with BUSTER-2.10.4 (39) using TLS group and NCS restraints when necessary. Inspection

of the density maps and manual rebuilding were performed using COOT (40). The three-dimensional models of agrocinopine D-like2 and agrocinopine C-like2 (agroC-like1', agroC-like3 and agroC-like4) were generated with the GRADE webserver (grade.globalphasing.com). Refinement details of each structure are shown in Tables 3, 4, S1 and S2. Molecular graphic images were generated using PyMOL (http://www.pymol.org).

Constructions of transcriptional fusions and measurement of *acc* operon promoter activity. eGFP transcriptional fusions were generated as follows. The promoter regions of *acc* operon from the strains C58 and S4 (namely P*acc*C58 and P*acc*S4) were amplified by PCR using the following primers: pAccC58F CGGGGGATCCACTAGCGCAGGCAAGATGAATTCCA and pAccC58R TTCTTCCTCCACTAGGCTTCCCTTCCAACAAGAAATGG for C58, pACCS4F CGGGGGATCCACTAGATTATGGGGTGGGGCAAAGA and pAccS4R TTCTTCCTCCACTAGTTATGAGCGATATCTATCGTGAATGG for S4. PCR product were cloned into pGEM-T Easy vectors prior to subcloning of the ClaI-SalI fragment into the reporter plasmid pOT1e (41) digested with the same enzymes. Constructions were confirmed by PCR using pOT1eF and pOT1eR primers. Reporter constructions (P*acc*C58 and P*acc*S4) were introduced into *A. fabrum* C58 and *A. vitis* S4 strains by electroporation, and gentamycin-resistant colonies were selected.
Expression of the promoter regions of *acc* operon was quantified in AB minimal medium containing succinate without or with L-arabinose-2-phosphate (2 mM) as inducer thanks to the pOT1e plasmid carrying an eGFP transcriptional fusion as previously described (33). Measurements were performed after 20 hours of incubation at 28°C. Fluorescence measurements were normalized by dividing them by the corresponding values of optical density at 600 nm. Each condition was performed with 3 technical replicates and two biological replicates.

Molecular dynamics. All-atom MD simulations were performed using version 2022.4 of the GROMACS (42) modeling package with the CHARMM36 force field (43), in explicit solvent using the TIP3P water model. Simulation models of apo forms of AccAC58 and AccABo542 and closed forms with the removed ligand of AccAC58 and AccABo542 were prepared from X-rays structures (PDB 4ZE8, 8C75, 8CKD and 9CAY, respectively). Each protein was placed in a dodecahedral box of size 95.3 Å to ensure boundaries of at least 10 Å around the protein. Long-range electrostatic interactions (distance cut-off of 12 Å) were calculated using the "Particle-mesh Ewald" method (44). The protein system was neutralized by adding 1 and 2 sodium ions to AccABo542 and AccAC58, respectively. The total number of atoms, including water molecules, was 63585, 68059, 62043 and 59778 in apo AccABo542, apo AccAC58, closed forms of AccAC58 and AccABo542 boxes, respectively. Each system was minimized using the Steepest Descent algorithm and equilibrated for 1000 ps under NVT conditions and then 1000 ps under NPT conditions, with a pressure of 1 bar and temperature of 300 K. The production phase was launched under the same NPT conditions extended for 300 ns. It should be noted that the "LINCS" algorithm (45) was used during the MD simulations to block vibrations of bonds involving a hydrogen atom with a heavy atom, with a use of 2 fs integration step. To characterize the structural movements of the proteins during the simulations, Root Mean Square Fluctuations (RMSF) were calculated over the entire dynamics at intervals of 10 ps. RMSF values were calculated on the different MD trajectories, considering only the backbone atoms (N, Ca, C, O). The reference conformation to perform the RMSD calculations (backbone to backbone) was the structure at t = 0 ns after minimization. MD simulation was performed on 40 nodes on Intel(R) Xeon(R) CPU ES-2640 v4 @ 2.40GHz 10 cores.

Acknowledgements. We acknowledge SOLEIL for provision of synchrotron radiation facilities (proposals ID 20140774, 20150780, 20160782, 20170872, 20191181) in using PROXIMA beamlines. We thank John Reader for providing agrocin 84. The authors also thank the CCRMN and the CCSM of the University Claude Bernard Lyon 1 for analytical support. We thank I2BC integrative bioinformatics core facility BIOI2 for the performance computing infrastructure. We also thank Paul Hooykaas and Alex Bos for providing the LBA288 strain (C58 cured of pTiC58 containing the pTiBo542).

Funding. AV, DF and SM were supported by CNRS and ANR-Blanc SENSOR (ANR-12-BSV8-0003-01/02/03). This work benefited from the I2BC crystallization and microcalorimetry platforms supported by FRISBI ANR-10-INSB-05-01. China Scholarship council is acknowledged for a PhD grant to SL.

Author contribution. MA, LS and YQ provided the agrocinopine and analogues compounds. TM, LV and JD performed the growth assays and bacteria competition. AV, AES, GD, PL, SS and SM performed the crystallography work. AV performed the fluorescence assays. MAN performed the microcalorimetry experiments. AV, GD, AGM and DF performed QS assays and conjugative transfer. FA and CP performed the molecular dynamics. SM wrote the manuscript. All the authors discussed the results and contributed to the writing of the manuscript.

Competing interests. The authors declare no competing interests associated with the manuscript.

Data Availability Statement. The findings of this study are supported by the data within the article and its supplementary materials. Additional information of MD simulations can be obtained by contacting the corresponding author SM. The atomic coordinates and structure factors have been deposited at the Protein Data Bank under 8C6W, 8C6Y, 8C75, 8C6C and 8C6U for the four apo AccABo542 WT and apo AccABo542-F145YG440Q mutant structures respectively; PDB 8CB9, 8CAY, 8CAW for AccABo542 WT in complex with D-glucose-2-phosphate, agrocinopine D-like2 and agrocin 84 respectively; PDB 8CDO for AccABo542-F145YG440Q mutant in complex with agrocinopine C-like; PDB 8CKD, 8CKE and 8CKO for AccAC58 in complex with agrocinopine A, agrocinopine D-like2 and agrocinopine C-like, respectively; PDB 8CI6, 8CHC, 8CH2, 8CH1, 8CH3 and 8CJU for AccAS4 in complex with D-glucose-2-phosphate, agrocinopine D-like2, L-arabinose-2-phosphate, agrocinopine A, agrocin 84 and agrocinopine C-like, respectively.

References

1. Nester EW. Agrobacterium: nature's genetic engineer. Front Plant Sci. 2014;5:730. doi.org/10.3389/fpls.2014.00730
2. Dessaux Y, Faure D. Niche Construction and Exploitation by Agrobacterium: How to Survive and Face Competition in Soil and Plant Habitats. Curr Top Microbiol Immunol. 2018;418:55-86. doi: 10.1007/82_2018_83
3. Pitzschke A, Hirt H. New insights into an old story: Agrobacterium-induced tumour formation in plants by plant transformation. EMBO journal. 2010;29(6):1021-32. doi.org/10.1038/emboj.2010.8
4. Chilton MD, Saiki RK, Yadav N, Gordon MP, Quetier F. T-DNA from Agrobacterium Ti plasmid is in the nuclear DNA fraction of crown gall tumor cells. Proc Natl Acad Sci USA. 1980;77(7):4060-4. doi.org/10.1073/pnas.77.7.4060

5. Gelvin SB. Agrobacterium-mediated plant transformation: the biology behind the "gene-jockeying" tool. Microbiology and molecular biology reviews : MMBR. 2003;67(1):16-37. doi.org/10.1128/mmbr.67.1.16-37.20
6. Schell J, Van Montagu M, De Beuckeleer M, De Block M, Depicker A, De Wilde M, et al. Interactions and DNA transfer between Agrobacterium tumefaciens, the Ti-plasmid and the plant host. Proc R Soc Lond B Biol Sci. 1979;204(1155):251-66. doi.org/10.1098/rspb.1979.0026
7. Savka MA, Farrand SK. Modification of rhizobacterial populations by engineering bacterium utilization of a novel plant-produced resource. Nature biotechnology. 1997;15(4):363-8. doi.org/10.1038/nbt0497-363
8. Oger P, Petit A, Dessaux Y. Genetically engineered plants producing opines alter their biological environment. Nat Biotechnol. 1997;15(4):369-72. doi.org/10.1038/nbt0497-369
9. Lang J, Vigouroux A, Planamente S, El Sahili A, Blin P, Aumont-Nicaise M, et al. Agrobacterium uses a unique ligand-binding mode for trapping opines and acquiring a competitive advantage in the niche construction on plant host. PLoS Pathog. 2014;10(10):e1004444. doi.org/10.1371/journal.ppat.1004444
10. El Sahili A, Li SZ, Lang J, Virus C, Planamente S, Ahmar M, et al. A Pyranose-2-Phosphate Motif Is Responsible for Both Antibiotic Import and Quorum-Sensing Regulation in Agrobacterium tumefaciens. PLoS Pathog. 2015;11(8):e1005071. doi.org/10.1371/journal.ppat.1005071
11. Dessaux Y, Petit A, Farrand SK, Murphy PJ. Opines and opine-like molecules involved in plant-Rhizobiaceae interactions. The Rhizobiaceae1998. p. 173-97. doi.org/10.1007/978-94-011-5060-6_9
12. Klapwijk PM, Scheulderman T, Schilperoort RA. Coordinated regulation of octopine degradation and conjugative transfer of Ti plasmids in Agrobacterium tumefaciens: evidence for a common regulatory gene and separate operons. J Bacteriol. 1978;136(2):775-85. doi.org/10.1128/jb.136.2.775-785.19
13. Chilton WS, Chilton MD. Mannityl opine analogs allow isolation of catabolic pathway regulatory mutants. J Bacteriol. 1984;158(2):650-8. doi.org/10.1128/jb.158.2.650-658.1984
14. Tate ME, Murphy PJ, Roberts WP, Keer A. Adenine N6-substituent of agrocin 84 determines its bacteriocin-like specificity. Nature. 1979;280(5724):697-9. doi.org/10.1038/280697a0
15. Chopra S, Palencia As, Virus C, Tripathy A, Temple BR, Velazquez-Campoy A, et al. Plant tumour biocontrol agent employs a tRNA-dependent mechanism to inhibit leucyl-tRNA synthetase. Nature communications. 2013;4:1417. doi.org/10.1038/ncomms2421
16. Kim J-G, Park BK, Kim S-U, Choi D, Nahm BH, Moon JS, et al. Bases of biocontrol: sequence predicts synthesis and mode of action of agrocin 84, the Trojan horse antibiotic that controls crown gall. Proceedings of the National Academy of Sciences of the United States of America. 2006;103(23):8846-51. doi.org/10.1073/pnas.0602965103
17. Reader JS, Ordoukhanian PT, Kim J-g, Hwang I, Farrand S. Major Biocontrol of Plant Tumors. Science. 2005;309(5740):1533. doi: 10.1126/science.1116841
18. Roberts WP, Tate ME, Kerr A. Agrocin 84 is a 6-N-phosphoramidate of an adenine nucleotide analogue. Nature. 1977;265(5592):379-81. doi.org/10.1038/265379a0
19. Thompson RJ, Hamilton RHH, Pootjes CFF. Purification and characterization of agrocin 84. Antimicrobial agents and chemotherapy. 1979;16(3):293-6. doi.org/10.1128/aac.16.3
20. Wetzel ME, Olsen GJ, Chakravartty V, Farrand SK. The repABC Plasmids with Quorum-Regulated Transfer Systems in Members of the Rhizobiales Divide into Two Structurally and Separately Evolving Groups. Genome Biol Evol. 2015;7(12):3337-57. doi.org/10.1093/gbe/evv227
21. Zhang Q, Li SZ, Ahmar M, Soulere L, Queneau Y. Esters of Glucose-2-Phosphate: Occurrence and Chemistry. Molecules. 2020;25(12). doi.org/10.3390/molecules25122829
22. Slater SC, Goldman BS, Goodner B, Setubal JC, Farrand SK, Nester EW, et al. Genome sequences of three agrobacterium biovars help elucidate the evolution of multichromosome genomes in bacteria. J Bacteriol. 2009;191(8):2501-11. doi.org/10.1128/jb.01779-08
23. Hooykaas MJG, Shao S, Hooykaas PJJ. Characterization of the Agrobacterium octopine-cucumopine catabolic plasmid pAtAg67. Plasmid. 2022;121:102629. DOI: 10.1016/j.plasmid.2022.102629

24. Berntsson RPa, Smits SHJ, Schmitt L, Slotboom D-J, Poolman B. A structural classification of substrate-binding proteins. FEBS letters.584(12):2606-17. doi.org/10.1016/j.febslet.2010.04.043
25. Grandclement C, Tannieres M, Moréra S, Dessaux Y, Faure D. Quorum quenching: role in nature and applied developments. FEMS Microbiol Rev. 2016;40(1):86-116. doi: 10.1093/femsre/fuv038
26. Burr TJ, Bazzi C, Sule S, Otten L. Crown Gall of Grape: Biology of Agrobacterium vitis and the Development of Disease Control Strategies. Plant Dis. 1998;82(12):1288-97. doi:10.1094/PDIS.1998.82.12.1288
27. Padilla R, Gaillard V, Le TN, Bellvert F, Chapulliot D, Nesme X, et al. Development and validation of a UHPLC-ESI-QTOF mass spectrometry method to analyze opines, plant biomarkers of crown gall or hairy root diseases. J Chromatogr B Analyt Technol Biomed Life Sci. 2021;1162:122458. doi: 10.1016/j.jchromb.2020.122458
28. Lindberg M, Oscarson, S. Synthesis of D-Glucos-2-yl Sucros-2-yl Phosphate (Agrocinopin C) and bis (D-glycos-2-yl) phosphate (agrocinopin D). J Carbohydr Chem. 1993;11:243-53. doi.org/10.1080/07328309308020123
29. Asenstorfer RE, Ryder MH, Jones GP. Agrocinopine C, a Ti-plasmid-coded enzyme-product, is a 2-O, 6-O linked phosphodiester of D-Glucose and sucrose. Phytochemistry. 2022;194:113013. DOI: 10.1016/j.phytochem.2021.113013
30. Queneau Y, Jarosz S, Lewandowski B, Fitremann J. Sucrose chemistry and applications of sucrochemicals. Adv Carbohydr Chem Biochem. 2007;61:217-92. doi.org/10.1016/S0065-2318(07)61005-1
31. de Boer M, Gouridis G, Vietrov R, Begg SL, Schuurman-Wolters GK, Husada F, et al. Conformational and dynamic plasticity in substrate-binding proteins underlies selective transport in ABC importers. Elife. 2019;8. doi.org/10.7554/eLife.44652
32. Lichtenthaler F.W. IS, Pokinskyj P. Selective 2-*O*-benzylation of Sucrose: A facile Entry to its 2-Deoxy- and 2-Keto-Derivatives and to Sucrosamine. Liebigs Ann 1995;1995:1939-47. https://doi.org/10.1002/jlac.1995199511273
33. Meyer T, Renoud S, Vigouroux A, Miomandre A, Gaillard V, Kerzaon I, et al. Regulation of Hydroxycinnamic Acid Degradation Drives Agrobacterium fabrum Lifestyles. Mol Plant Microbe Interact. 2018;31(8):814-22. DOI: 10.1094/MPMI-10-17-0236-R
34. Cha C, Gao P, Chen YC, Shaw PD, Farrand SK. Production of acyl-homoserine lactone quorum-sensing signals by gram-negative plant-associated bacteria. Molecular plant-microbe interactions : MPMI. 1998;11(11):1119-29. DOI: 10.1094/MPMI.1998.11.11.1119
35. Wiseman T, Williston S, Brandts JF, Lin LN. Rapid measurement of binding constants and heats of binding using a new titration calorimeter. Anal Biochem. 1989;179(1):131-7. DOI: 10.1016/0003-2697(89)90213-3
36. Kabsch W. XDS. Acta crystallographica Section D, Biological crystallography.66(Pt 2):125-32. doi: 10.1107/S0907444909047337
37. Vonrhein C, Flensburg C, Keller P, Sharff A, Smart O, Paciorek W, et al. Data processing and analysis with the autoPROC toolbox. Acta Crystallogr D Biol Crystallogr. 2011;67(Pt 4):293-302. DOI: 10.1107/S0907444911007773
38. McCoy AJ, Grosse-Kunstleve RW, Adams PD, Winn MD, Storoni LC, Read RJ. Phaser crystallographic software. J Appl Crystallogr. 2007;40(Pt 4):658-74. DOI: 10.1107/S0021889807021206
39. Blanc E, Roversi P, Vonrhein C, Flensburg C, Lea SM, Bricogne G. Refinement of severely incomplete structures with maximum likelihood in BUSTER-TNT. Acta crystallographica Section D, Biological crystallography. 2004;60(Pt 12 Pt 1):2210-21. doi.org/10.1107/S0907444904016427
40. Emsley P, Cowtan K. Coot: model-building tools for molecular graphics. Acta Crystallogr D Biol Crystallogr. 2004;60(Pt 12 Pt 1):2126-32. DOI: 10.1107/S0907444904019158
41. Allaway D, Schofield NA, Leonard ME, Gilardoni L, Finan TM, Poole PS. Use of differential fluorescence induction and optical trapping to isolate environmentally induced genes. Environ Microbiol. 2001;3(6):397-406. DOI: 10.1046/j.1462-2920.2001.00205.x

42. Abraham MJ, Murtola T, Schulz R., Páll S., Smith J. C., Hess B., et al. GROMACS: High performance molecular simulations through multi-level parallelism from laptops to supercomputers. SoftwareX. 2015;1-2:19-25. doi.org/10.1016/j.softx.2015.06.001
43. Huang J, Rauscher S, Nawrocki G, Ran T, Feig M, de Groot BL, et al. CHARMM36m: an improved force field for folded and intrinsically disordered proteins. Nat Methods. 2017;14(1):71-3. DOI: 10.1038/nmeth.4067
44. Darden T, York D, Pedersen L. Particle mesh Ewald: An W log(N) method for Ewald sums in large systems. J Chem Phys. 1993;98:10089-92. doi.org/10.1063/1.464397
45. Hess B. P-LINCS: A Parallel Linear Constraint Solver for Molecular Simulation J Chem Theory Comput. 2008, 4:116-122. doi: 10.1021/ct700200b
46. Gouet P, Courcelle E, Stuart DI, Metoz F. ESPript: analysis of multiple sequence alignments in PostScript. Bioinformatics. 1999;15(4):305-8. DOI: 10.1093/bioinformatics/15.4.305

Figures legends

Figure 1. Representation molecules and transport of agrocinopines. (**A**) L-arabinose-2-phosphate, D-glucose-2-phosphate, agrocinopines A, B, C and D, an analogue of agrocinopines D (AgroD-like2) and agrocin 84. (**B**) A simplified schematic representing the transport of agrocinopines from transformed plant cells by the strains C58 (producing agrocinopines A/B) or Bo542 (producing agrocinopines C/D) into agrobacteria. All the genes allowing the synthesis of agrocinopines are located on the T-DNA from the pTi incorporated into the plant genome. In *A. fabrum* C58 and *A. tumefaciens* Bo542, the *acc*ABCDE genes are located on the Ti plasmid and code for agrocinopine import. The strain C58 can uptake the four agrocinopines A/B/C/D whereas the strain Bo542 seems to transport its own agrocinopines C/D only. The green triangles in agrocinopines A/B represent the L-arabinose-2-phosphate while the blue ones in agrocinopines C/D represent the D-glucose-2-phosphate. The rest of the molecule is either a sucrose or a sugar.

Figure 2. Growth assays. During 2 days, OD_{600nm} of *A. fabrum* C58 (containing pTiC58, pink line) and *A. tumefaciens* Bo542 (blue line) was measured in AB minimal medium supplemented with D-glucose-2-phosphate (**A**), agrocinopine D-like2 (**B**), L-arabinose-2-phosphate (**C**), agrocinopine A (**D**), succinate (**E**) as carbon sources. Similarly, OD_{600nm} of C58, C58 lacking the pTi plasmid (referred to as C103), C58 cured of both pTi and pAt (referred to as C58:00), and C58pTiBo542 (cured of pTiC58 and containing the pTiBo542, referred to as LBA288) was also measured in AB minimal medium supplemented with D-glucose-2-phosphate (**F**). Growth curves correspond to the mean from two biological replicates and four technical replicate.

Figure 3. Quantification of OC8HSL production and Ti plasmid conjugation. Induction was performed by L-arabinose-2-phosphate, D-glucose-2-phosphate, agrocinopine A and agrocinopine D-like2 in the strain Bo542. *A. tumefaciens* C58.00 was used as donor cells. Results were obtained after 96 h of culture. SDs correspond to biological replicates. OC8HSL was not detected for agrocinopine A and L-arabinose-2-phosphate. Experiments independently repeated three times produced similar results.

Figure 4. The strain containing pTiC58 outcompetes the strains harboring pTiBo542 in D-glucose-2-phosphate supplemented medium. Proportion (in %) of C58 (in black) and Bo542 or LBA288 (in white) strains are indicated in the starter inoculum, in YPG medium and in D-glucose-2-phosphate supplemented AB medium after 36 hours of culture. Asterisks indicate significant differences (student test (p-value = 0.05)) whereas NS means no significant differences between conditions. Proportions were calculated from two independent assays with five technical replicates.

Figure 5. **Structures of unliganded and liganded AccABo542 and AccAC58 and comparison**. Ribbon representation of apo AccABo542 (PDB 8C75) in deepteal and cyan colors for lobes 1 (residues 31-280 and 495-521) and 2 (residues 284-491), respectively. The short hinge region is shown in gold. (**A**), and structural comparison with apo AccAC58 shown in pink (PDB 4ZE8) (**B**). Ribbon representation of AccABo542-G2P complex (PDB 8CB9) colored as in **A**, the G2P bound between the two lobes is in red sticks (**C**). Structural comparison between the open unliganded (cyan, PDB 8C75) and the closed liganded (blue, PDB 8CB9) forms of AccABo542 with their lobes 1 superimposed. G2P is shown in red sticks (**D**). Ligand-binding site of AccABo542 showing protein residues as cyan sticks involved in the ligand binding in the same orientation as in **C**. Hydrogen bonds are shown as dashed lines in black and red, for distances up to 3.2 Å and 3.4 Å, respectively. G2P is in blue (PDB 8CB9) (**E**) and AgroD-like2 is in magenta (PDB 8CAY) (**F**). Ligand-binding site of AccAC58 showing protein residues as pink sticks involved in the ligand binding. Hydrogen bonds are shown as dashed lines in black and red, for distances below 3.2 Å and 3.4 Å, respectively. AgroD-like2 is in magenta (PDB 8CKD) (**G)** and G2P is in blue (PDB 4RA1) (**H**). Superimposition of the ligand binding sites of AccABo542 (cyan) and AccAC58 (pink) in complex with G2P (blue) (**I**) and AgroD-like2 (magenta) (**J**). Phe145 in AccABo542 is not conserved and shown in gray stick. Each ligand is shown in its Fo-Fc omit map contoured at 4σ in the same orientation as bound to the protein. P and Glc labels are for Phosphate and Glucose, respectively (**E**, **F** and **G**).

Figure 6. **Agrocin 84 bound to the binding site of AccA**. AccABo542 (**A**), AccAC58 (**B**) and AccAS4 (**C**). Amino acids and agrocin 84 are shown as stick. Each ligand is shown in its Fo-Fc omit map contoured at 3σ. TM84, P, Glc, labels are for Toxic Moiety 84, Phosphoramidate and Glucose, respectively. Hydrogen bonds of the TM84 moiety of agrocin 84 are shown as dashed lines in black for distances up to 3.2 Å. (**D**), Comparison of the bound agrocin 84 shown in cyan, pink and light-orange sticks in AccABo542, AccAC58 and AccAS4, respectively, when the three protein-agrocin 84 complexes are superimposed.

Figure 7. Model of L-arabinose-2-phosphate bound to the binding site of AccABo542. (**A**) Superposition of the L-arabinose-2-phosphate (green) bound to AccAC58 (PDB 4ZEI) on the D-glucose-2-phosphate (blue) bound to AccABo542 shown as stick. (**B**) A modeled L-arabinose-2-phosphate (green) bound to the binding site of AccABo542, between the lobes 1 and 2 residues shown as deep teal and cyan sticks, respectively. Hydrogen bonds between the modeled L-arabinose-2-phosphate (green) and AccABo542 are shown as dashed lines in black and red for distances up to 3.2 Å and 3.4 Å, respectively. L-arabinose-2-phosphate bound to AccAC58 (PDB 4ZEI) (**C**) and AccAS4 (PDB 8CH2) (**D**).

Figure 8. Structure-based sequence alignment of the three studied AccA. The secondary structure elements are labeled and indicated by coils for α-helices, arrow for β-strands and η for short 3_{10} helices. Similar residues are in red and identical residues are shown as white letters on a red background. The positions of the 25 residues involved in agrocinopines/agrocin 84 recognition by polar and hydrophobic interactions are indicated by red triangles for the conserved ones, by orange triangles for the non-conserved ones, and by green triangles, those conserved in AccAC58/AccAS4 and not in AccABo542. Phe145 and Gly440 were mutated. The figure was created using ESPript 3.0 (https://espript.ibcp.fr/ESPript/ESPript/) (46) from CLUSTAL OMEGA (https://www.ebi.ac.uk/Tools/msa/clustalo).

Figure 9. Agrocinopine C-like bound to the binding site of AccA. Analogues of agrocinopine C-like2 obtained from the synthesis namely AgroC-like1', AgroC-like3 and AgroC-like4 (**A**). AgroC-like1' in AccABo542 (**A**), AgroC-like3 in AccAC58 (**B**) and AgroC-like4 in AccAS4 (**C**). Amino acids and agrocinopine C-like are shown as stick. Each ligand is shown in its Fo-Fc omit map contoured at 4σ. Rib, P, Glc, labels are for Ribose, Phosphate and Glucose, respectively. Hydrogen bonds of the sucrose moiety of agrocinopine C-like are shown as dashed lines in black for distances up to 3.2 Å (**D**), Comparison of the bound AgroC-like1', AgroC-like3 and AgroC-like4 shown in cyan, pink and light-orange sticks to AccABo542, AccAC58 and AccAS4, respectively, when the three protein-ligand complexes are superimposed.

Figure 10. Molecular dynamics of AccABo542 and AccAC58. RMSF comparison between apo AccAC58 and apo AccABo542 (**A**), between the apo and closed forms of AccAC58 (**B**) and between the apo and closed forms of AccABo542 (**C**). The five flexible regions in apo AccAC58 compared to apo AccABo542 are defined by 5 colored boxes in the RMSF analysis: residues 48-60 (blue), 89-103 (green), 325-352 (red), 414-445 (orange) and 450-483 (purple) (**A**) These five regions are highlighted in the same color code in the two ribbon representations of apo AccAC58 in **D** (front view) and in 180° rotation in **E** (back view). The surface of the ligand binding site is shown in gray.

Table 1. Melting temperature *Tm* measured by DSC (**A**) and thermal unfolding *Ti* measured by nanoDSF (**B**) of AccABo542 and AccAC58 and effect of agrocinopine or derivatives. DSC and nanoDSF experiments were performed twice.

A	***Tm* (°C)**	***ΔTm***	**ΔH_1 (kcal/mol)**	**ΔHVH_1 (kcal/mol)**
AccABo542	63.82 ± 0.011		263	149
+ agrocinopine A	63.62 ± 0.011	-0.2	265	153
+ agrocinopine D-like2	66.65 ± 0.012	2.83	321	165
+ L-arabinose-2-phosphate	63.39 ± 0.010	-0.43	243	155
+ D-glucose-2-phosphate	64.06 ± 0.010	0.24	264	161
AccAC58	57.27 ± 0.010		353	171
+ agrocinopine A	62.05 ± 0.009	4.78	367	182
+ agrocinopine D-like2	66.60 ± 0.009	9.33	383	190
+ L-arabinose-2-phosphate	60.15 ± 0.009	2.88	341	178
+ D-glucose-2-phosphate	64.43 ± 0.008	7.16	377	181

B	***Ti* (°C)**	***ΔTi* (°C)**	**Initial Ratio**	**ΔRatio**
AccABo542	69.67 ± 0.09		0.7906	0.2552
+ agrocinopine A	69.88 ± 0.15	0.21	0.7933	0.2616
+ agrocinopine D-like2	75.89 ± 0.32	6.22	0.8149	0.2310
+ L-arabinose-2-phosphate	69.41 ± 0.06	-0.26	0.7941	0.2450
+ D-glucose-2-phosphate	74.33 ± 0.25	4.66	0.8966	0.1502
AccAC58	63.09 ± 0.20		0.6983	0.3095
+ agrocinopine A	72.06 ± 0.36	8.97	0.7299	0.2760
+ agrocinopine D-like2	76.61 ± 0.13	13.52	0.6997	0.3094
+ L-arabinose-2-phosphate	65.78 ± 0.02	2.69	0.8030	0.2020
+ D-glucose-2-phosphate	74.68 ± 0.25	11.59	0.7868	0.2603

Table 2. Affinity values of AccABo542 and AccAC58 towards D-glucose-2-phosphate and agrocinopine D-like2 measured by autofluorescence and ITC. ITC and fluorescence experiments were performed twice and done on triplicate, respectively.

	Fluo	**ITC**				
	K_D **(µM)**	**n**	K_D **(µM)**	ΔH **(kcal/mol)**	$-T\Delta S$ **(kcal/mol)**	ΔG **(kcal/mol)**
AccABo542-D-glucose-2-phosphate	15.03 ± 0.87	0.9	9.67 ± 1.37	-6.87	0.03	-6.84
AccABo542-agrocinopine D-like2	1.60 ± 0.10	1.06	1.76 ± 0.10	-11.6	3.7	-7.9
AccAC58-D-glucose-2-phosphate	1.25 ± 0.06	1.06	0.42 ± 0.04	-9.6	0.9	-8.7
AccAC58-agrocinopine D-like2	0.12 ± 0.01	1.08	0.08 ± 0.01	-10.8	1.1	-9.7

Table 3. Crystallographic data and refinement parameters of apo AccABo542 wild-type and F144YG440Q mutant.

apo AccABo542	**Form 1**	**Form 2**	**Form 3**	**Form 4**	**Mutant-Form 4**
PDB code	**8C6W**	**8C6Y**	**8C75**	**8C6R**	**8C6U**
Crystallization conditions	**A:** 30% PEG 4K, 0.1 M Tris-HCl pH 8	**B:** 30% PEG 4K, AcNH4, Na citrate pH 5.6	**B**	**B**	**B**
Za	2	1	2	1	1
Space group Cell parameters (Å,°)	$P2_12_12_1$ *a*= 91.7 *b*= 100.6 *c*= 116.0	$P2_12_12_1$ *a*= 47.9 *b*= 58.9 *c*= 177.8	P21 *a*= 47.0 *b*= 182.07 *c*= 58.6 *β*= 94.1	$P2_12_12_1$ *a*= 53.3 *b*= 59.3 *c*= 181.4	$P2_12_12_1$ *a*= 53.2 *b*= 60.0 *c*= 181.2
Resolution (Å)	49.03-2.8 (2.87-2.8)	49.19-1.9 (1.95-1.90)	49.19-1.66 (1.71-1.66)	85.8-1.88 (2.14-1.88)	45.92-1.84 (1.89-1.84)
Estimated resolution limit (Å). STARANISO	2.8, 2.8 2.84	2.5, 1.94, 1.9	1.95, 1.66, 1.77	3.2, 1.67, 1.73	2.49, 1.84, 2.15
No. of observed reflections	323554 (22361)	574539 (41625)	606098 (37747)	641728 (33178)	647353 (39682)
No. of unique reflections	27072 (1963)	40544 (2912)	113578 (7440)	47558 (2378)	51418 (3718)
Completeness (%)	85.7 (26.0)	66.9 (14.5)	74.0 (7.1)	46.2 (7.3)	61.9 (4.9)
R_{merge}(%)	34.3 (162.2)	18.8 (183.2)	11.1 (117.7)	14 (153.3)	21.3 (164.3)
R_{pim} (%)	11.8 (95.2)	7.2 (161.4)	6.1(125.7)	9.1 (201.5)	8.7 (217.1)
$I/\sigma(I)$	7.3 (1.7)	11.0 (1.4)	9.3 (1.4)	12.5 (1.7)	9.8 (1.3)
$CC_{1/2}$	0.994 (0.678)	0.998 (0.580)	0.997 (0.440)	0.998 (0.587)	0.997 (0.356)
R_{cryst} (%)	22.8	21.8	21.9	20.8	23.4
R_{free} (%)	26.5	26.1	25.6	25	28.4
rms bond deviation (Å)	0.005	0.009	0.009	0.009	0.009
rms angle deviation (°)	0.76	1.04	1.09	1.05	1.04
Average B ($Å^2$) Protein A/B solvent	 50.5/51.3 27.5	 25.8 30.7	 32.3/31.9 35.2	 42.8 37.3	 29.7 32.2
[a]Clashscore MolProbity score	3.69 1.68	0.77 1.04	1.6 1.13	1.28 1.10	1.15 1.01
[a]Ramachandran plot (%) Favored Outliers	 94.58 0	 97.34 0	 96.83 0	 96.32 0	 96.93 0

Values for the highest resolution shell are in parentheses.
$CC_{1/2}$ = percentage of correlation between intensities from random half-dataset.
[a]Calculated with MolProbity
STARANISO applies ellipsoidal mask: estimated resolution limits along the three crystallographic directions *a**, *b**, *c**.

Table 4 Crystallographic data and refinement parameters for liganded AccABo542 wild-type and F144YG440Q mutant.

AccABo542	**D-glucose-2-phosphate**	**agrocinopine D-like2**	**agrocin 84**	**Mutant-agrocinopine C-like1'**
PDB code	**8CB9**	**8CAY**	**8CAW**	**8CDO**
Space group Cell parameters (Å,°)	$P2_12_12_1$ *a*= 42.9 *b*= 59.2 *c*= 183.3	C2 *a*= 107.1 *b*= 40.2 *c*= 103.4 *β*= 114.4	C2 *a*= 104.1 *b*= 51.1 *c*= 102.1 *β*= 109.1	$P2_13$ *a*=*b*=*c*= 122.2
Resolution (Å)	91.6-1.79 (1.92-1.79)	53.2-1.62 (1.78-1.62)	49.2-1.25 (1.27-1.25)	86.3-1.32 (1.36-1.32)
Estimated resolution limit (Å) STARANISO	2.38, 1.76, 1.74	1.62, 1.94, 1.77	1.41, 1.52, 1.25	
No. of observed reflections	499522 (10006)	188189 (9951)	436693 (8191)	5541034 (273836)
No. of unique reflections	43037 (1616)	50253 (2610)	119897 (3461)	135341 (6758)
Completeness (%)	71.7 (18.8)	70.6 (14.7)	88.9 (64.5)	95.6 (54.4)
R_{merge} (%)	7.4 (122.1)	21.1 (70.1)	6.2 (76.1)	10.2 (327.1)
R_{pim} (%)	2.2 (50.8)	13.5 (42.8)	3.6 (47)	1.6 (51.9)
$I/\sigma(I)$	16.3 (1.2)	7.48 (1.7)	12.2 (1.9)	23.3 (1.4)
$CC_{1/2}$	0.999 (0.527	0.7 (0.629)	0.998 (0.565)	1 (0.635)
R_{cryst} (%)	22.8	19.6	16.9	14.7
R_{free} (%)	27.1	22.6	19.1	16.8
rms bond deviation (Å)	0.009	0.010	0.013	0.012
rms angle deviation (°)	1.05	1.1	1.22	1.16
Average *B* (Å^2) Protein Ligand Solvent	 45.4 25.6 36.7	 25.4 21.6 30.8	 20.4 30.5 36.6	 20.5 19.5 35.3
[a]Clashscore MolProbity score	1.68 1.17	2.17 1.28	1.13 1	1.36 1.03
[a]Ramachandran plot (%) Favored Outliers	 96.27 0	 96.52 0	 96.93 0	 97.05 0

Values for the highest resolution shell are in parentheses

$CC_{1/2}$ = percentage of correlation between intensities from random half-dataset

[a]Calculated with MolProbity

STARANISO applies an ellipsoidal mask: estimated resolution limits along the three crystallographic directions *a**, *b**, *c**.

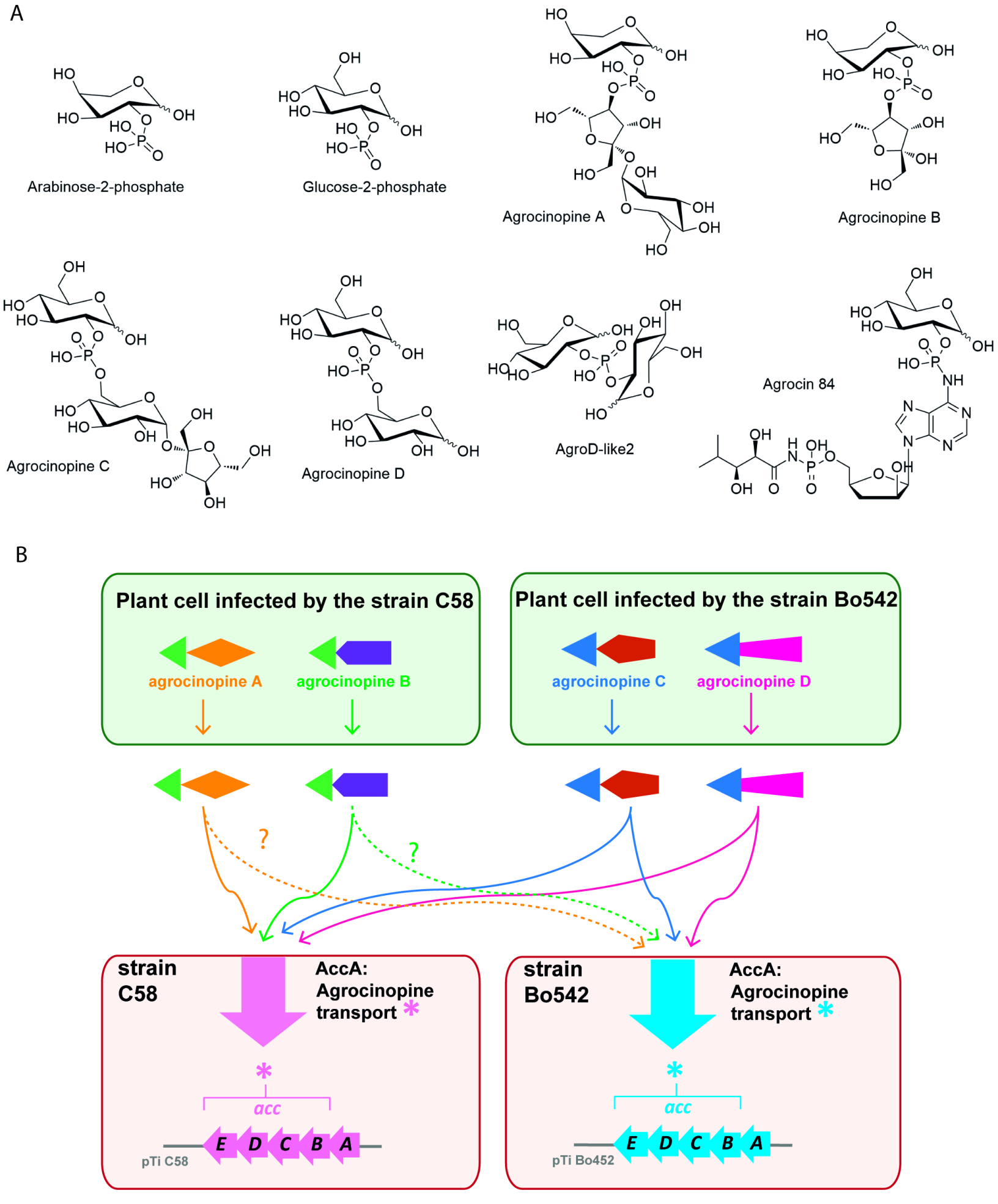
A
Arabinose-2-phosphate
Glucose-2-phosphate
Agrocinopine A
Agrocinopine B
Agrocinopine C
Agrocinopine D
AgroD-like2
Agrocin 84
B
Plant cell infected by the strain C58
agrocinopine A
agrocinopine B
Plant cell infected by the strain Bo542
agrocinopine C
agrocinopine D
?
?
strain C58
AccA: Agrocinopine transport *
*
acc
E D C B A
pTi C58
strain Bo542
AccA: Agrocinopine transport *
*
acc
E D C B A
pTi Bo452

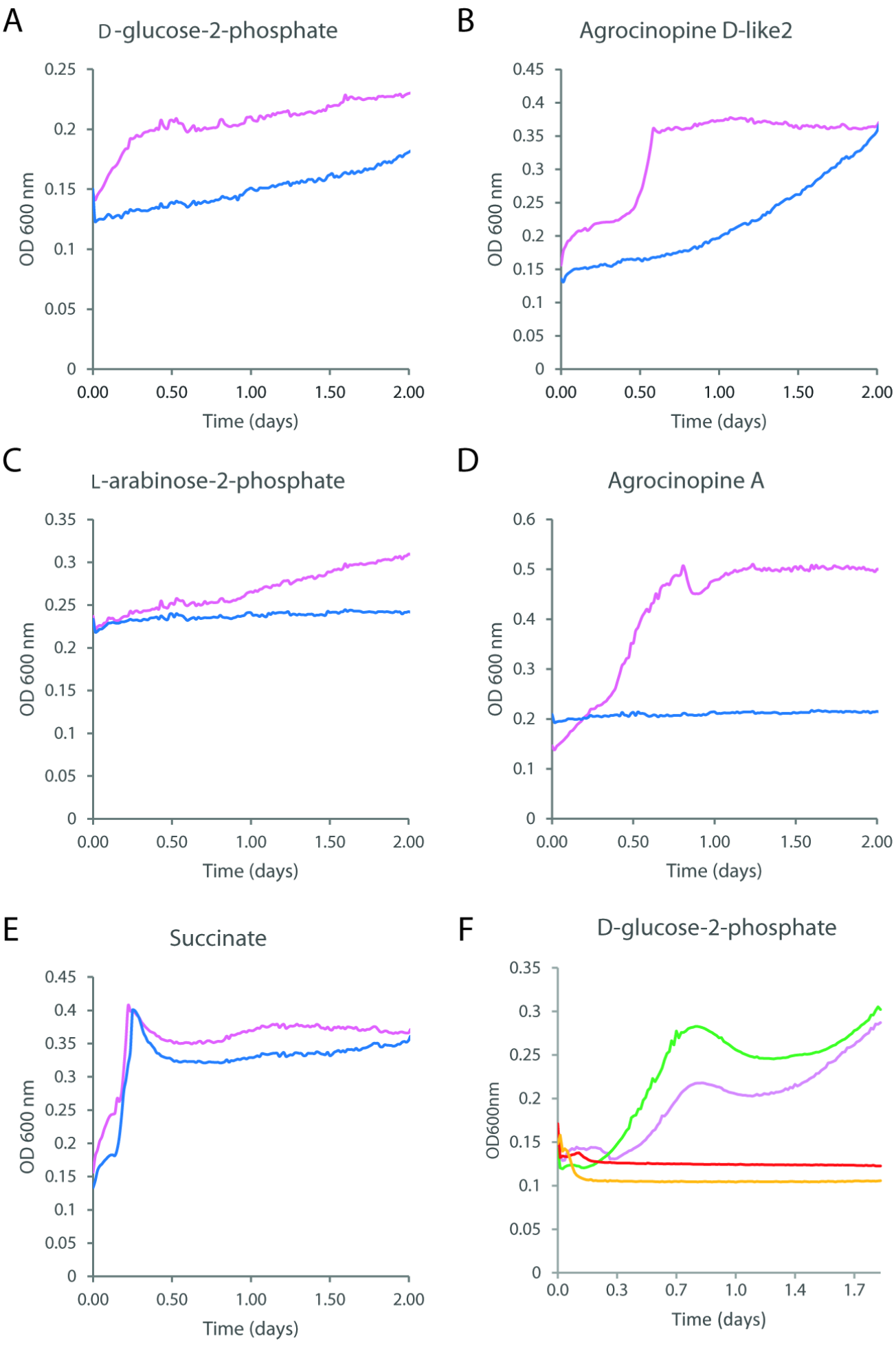
A
D-glucose-2-phosphate
OD 600 nm
Time (days)
B
Agrocinopine D-like2
OD 600 nm
Time (days)
C
L-arabinose-2-phosphate
OD 600 nm
Time (days)
D
Agrocinopine A
OD 600 nm
Time (days)
E
Succinate
OD 600 nm
Time (days)
F
D-glucose-2-phosphate
OD600nm
Time (days)
Bo542
C58
LBA288
C58:00
C103

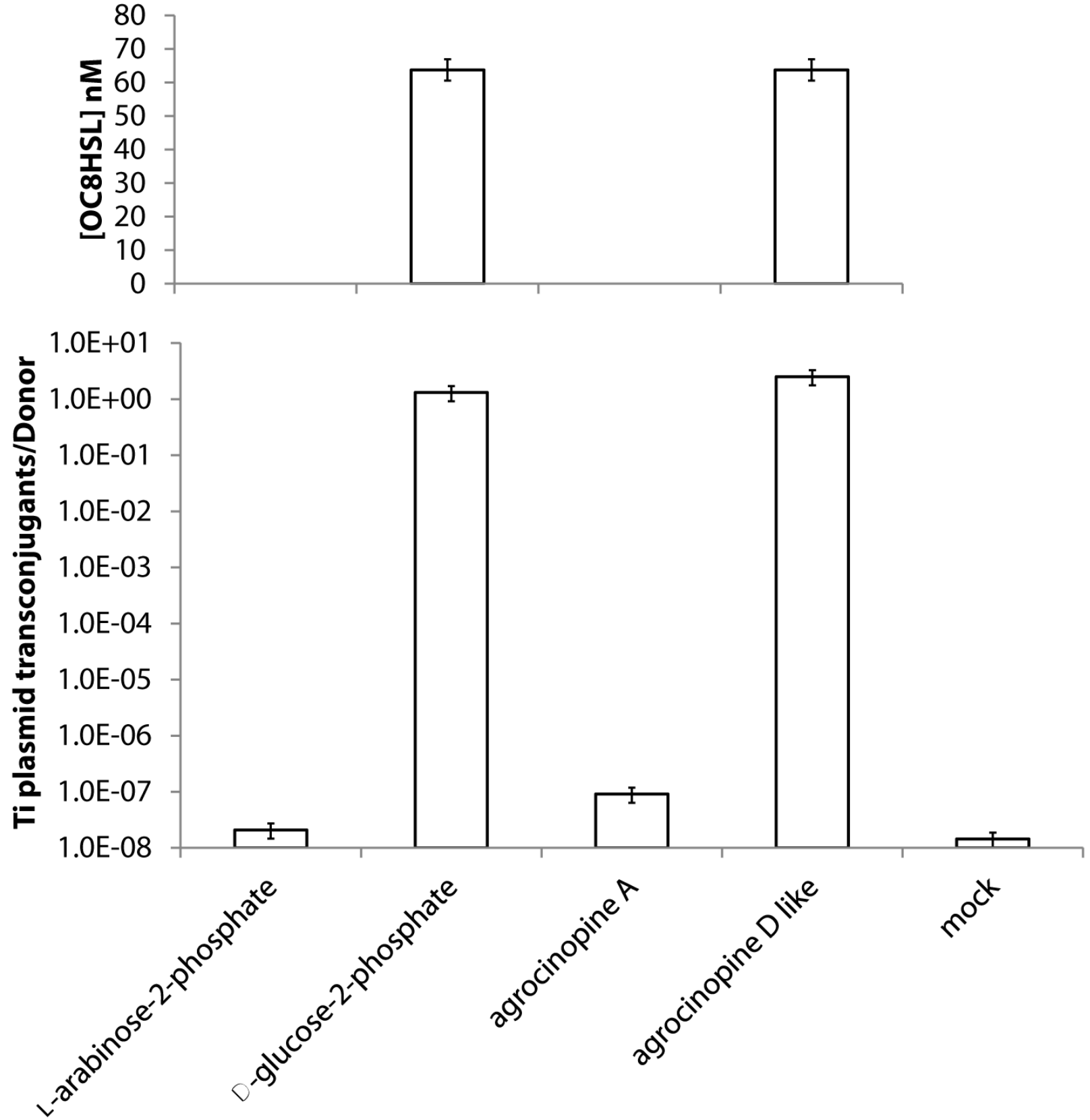
[OC8HSL] nM
80
70
60
50
40
30
20
10
0
Ti plasmid transconjugants/Donor
1.0E+01
1.0E+00
1.0E-01
1.0E-02
1.0E-03
1.0E-04
1.0E-05
1.0E-06
1.0E-07
1.0E-08
L-arabinose-2-phosphate
D-glucose-2-phosphate
agrocinopine A
agrocinopine D like
mock

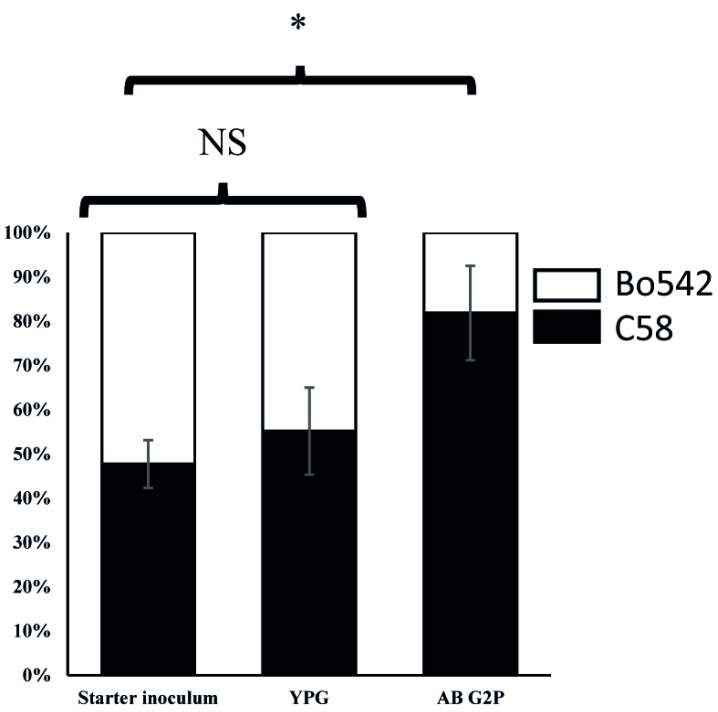
*
NS
100%
90%
80%
70%
60%
50%
40%
30%
20%
10%
0%
Starter inoculum
YPG
AB G2P
Bo542
C58

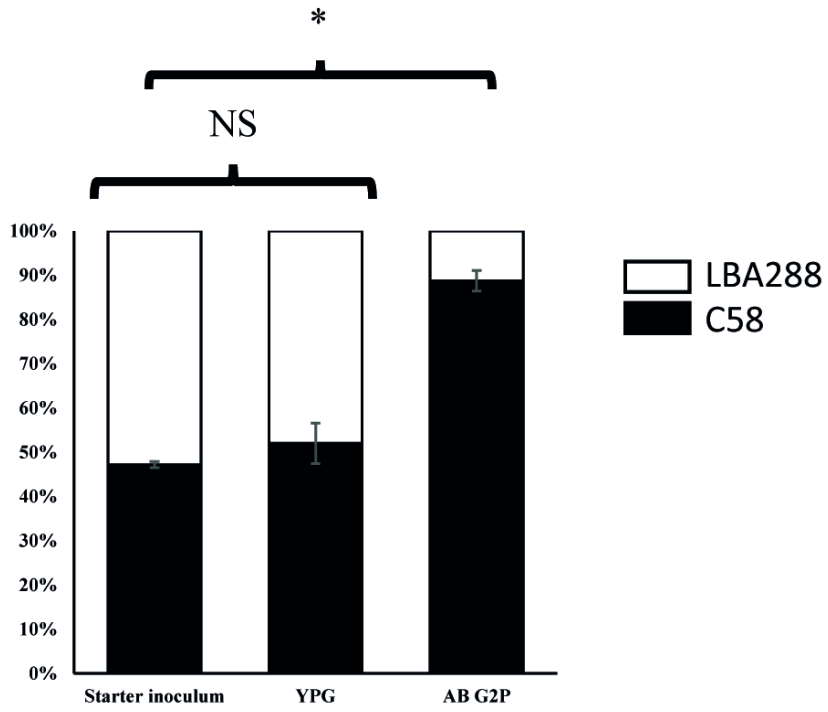
*
NS
100%
90%
80%
70%
60%
50%
40%
30%
20%
10%
0%
Starter inoculum
YPG
AB G2P
LBA288
C58

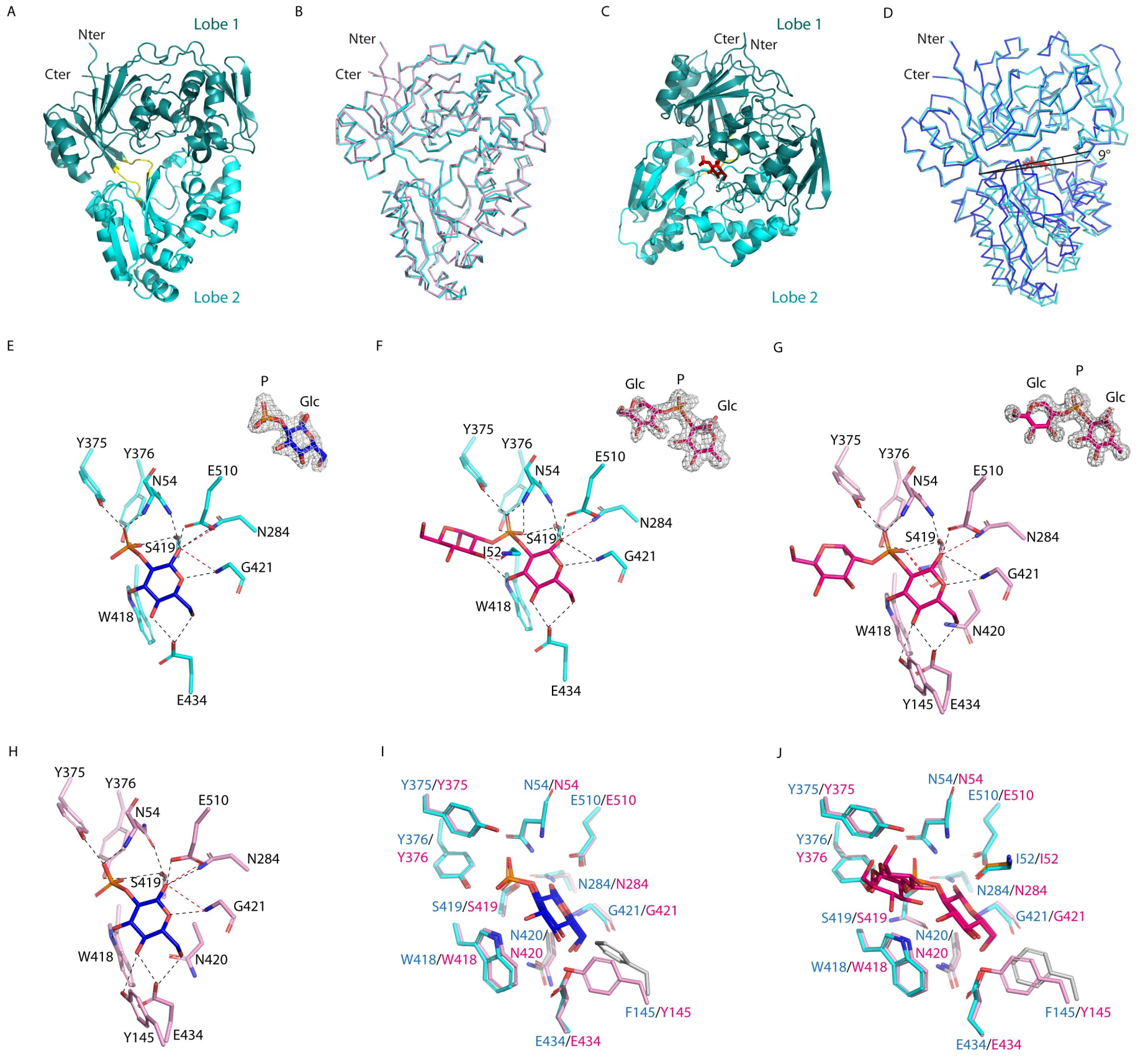
A
Lobe 1
Nter
Cter
Lobe 2
B
Nter
Cter
C
Lobe 1
Cter
Nter
Lobe 2
D
Nter
Cter
9°
E
P
Glc
Y375
Y376
N54
E510
N284
S419
G421
W418
E434
F
Glc
P
Glc
Y375
Y376
N54
E510
N284
S419
I52
G421
W418
E434
G
Glc
P
Glc
Y375
Y376
N54
E510
N284
S419
G421
W418
N420
Y145
E434
H
Y375
Y376
N54
E510
N284
S419
G421
W418
N420
Y145
E434
I
Y375/Y375
N54/N54
E510/E510
Y376/
Y376
N284/N284
S419/S419
G421/G421
N420/
N420
W418/W418
F145/Y145
E434/E434
J
N54/N54
Y375/Y375
E510/E510
Y376/
Y376
I52/I52
N284/N284
S419/S419
G421/G421
N420/
N420
W418/W418
F145/Y145
E434/E434

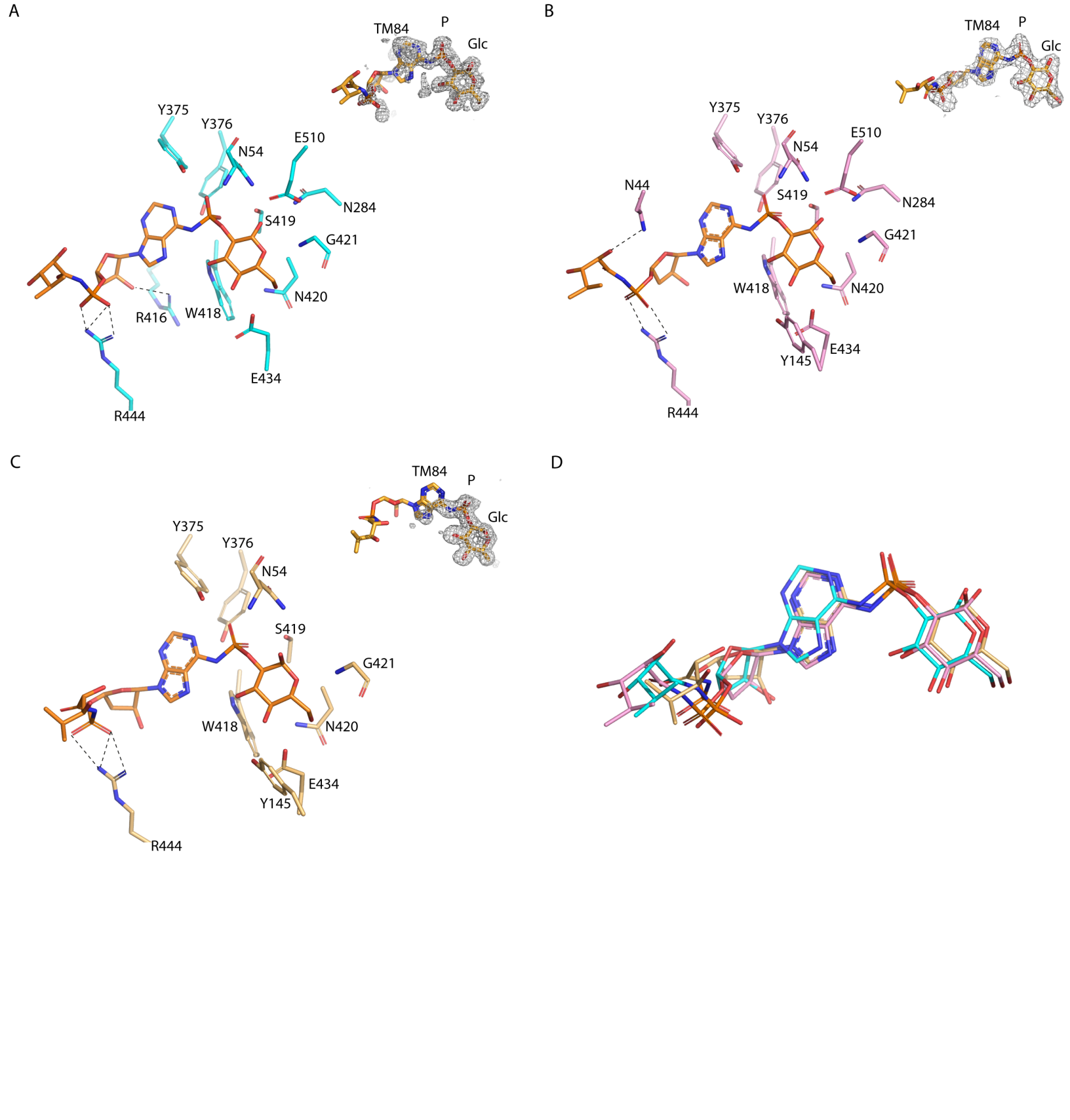
A
TM84
P
Glc
Y375
Y376
N54
E510
N284
S419
G421
N420
R416
W418
E434
R444
B
TM84
P
Glc
Y375
Y376
N54
E510
N44
S419
N284
G421
W418
N420
E434
Y145
R444
C
TM84
P
Glc
Y375
Y376
N54
S419
G421
W418
N420
E434
Y145
R444
D

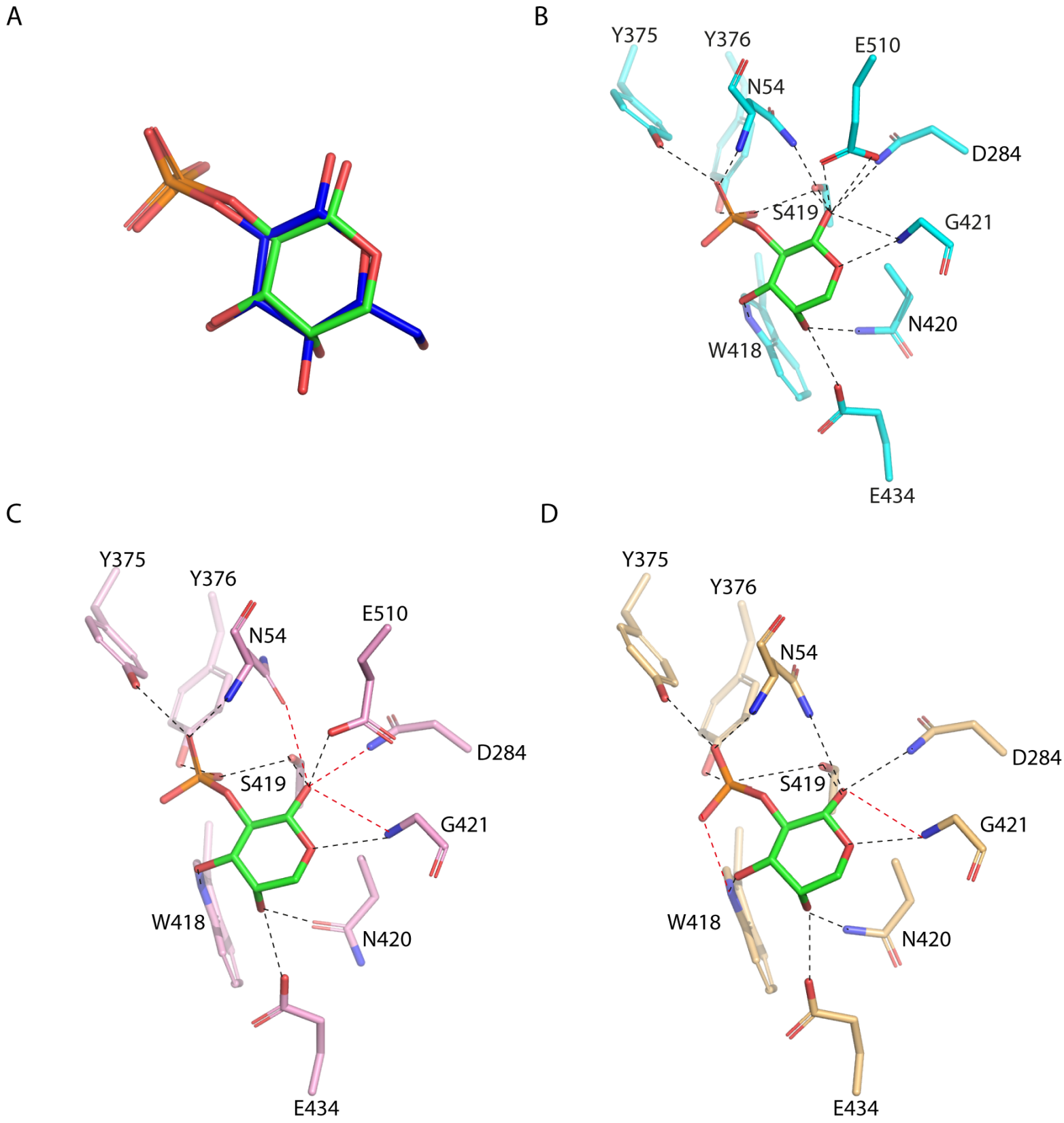
A
B
Y375
Y376
E510
N54
D284
S419
G421
N420
W418
E434
C
Y375
Y376
E510
N54
D284
S419
G421
W418
N420
E434
D
Y375
Y376
N54
D284
S419
G421
W418
N420
E434


Bo542-AccA
C58-AccA
S4-AccA

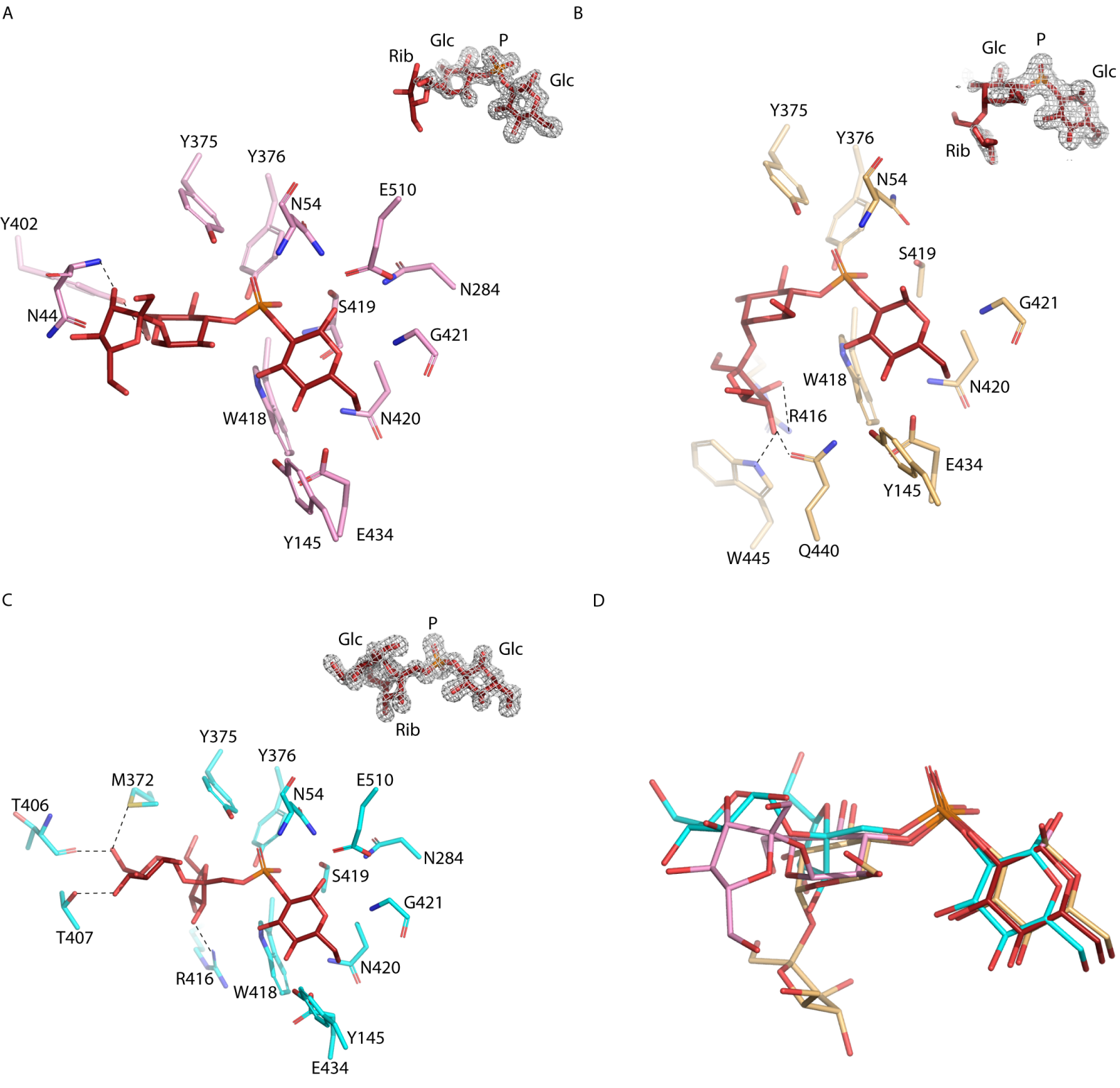
A
Glc
P
Rib
Glc
Y375
Y376
N54
E510
Y402
N284
N44
S419
G421
W418
N420
Y145
E434
B
Glc
P
Glc
Rib
Y375
Y376
N54
S419
G421
W418
N420
R416
E434
Y145
W445
Q440
C
P
Glc
Glc
Rib
Y375
Y376
M372
N54
E510
T406
N284
S419
G421
T407
N420
R416
W418
Y145
E434
D

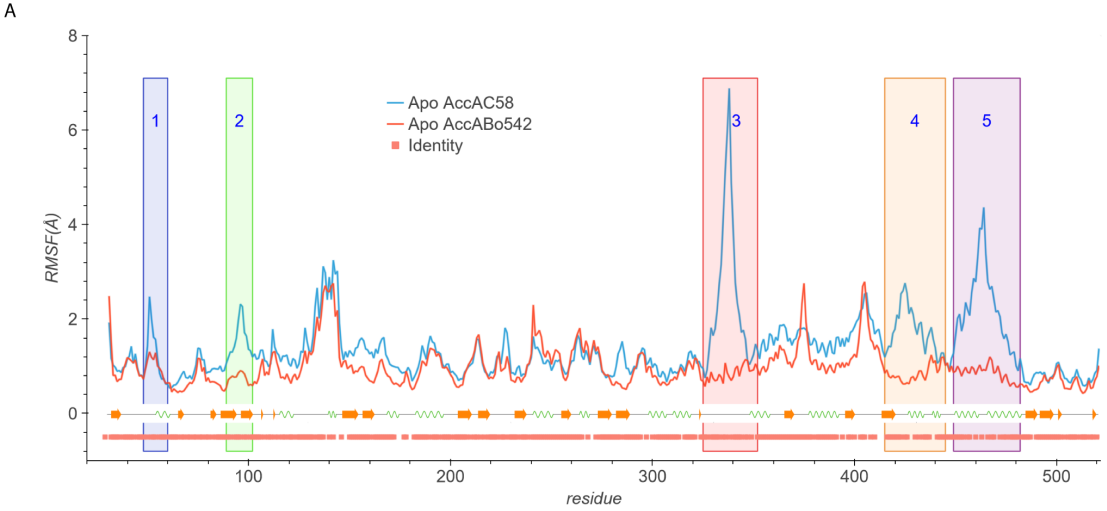
A
Apo AccAC58
Apo AccABo542
Identity
RMSF(Å)
residue
1
2
3
4
5

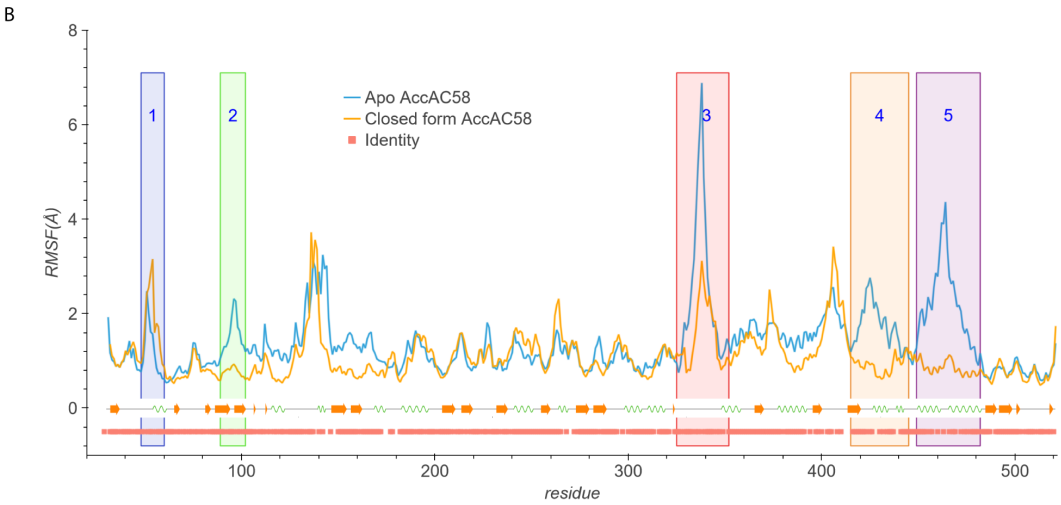
B
Apo AccAC58
Closed form AccAC58
Identity
RMSF(Å)
residue
1
2
3
4
5

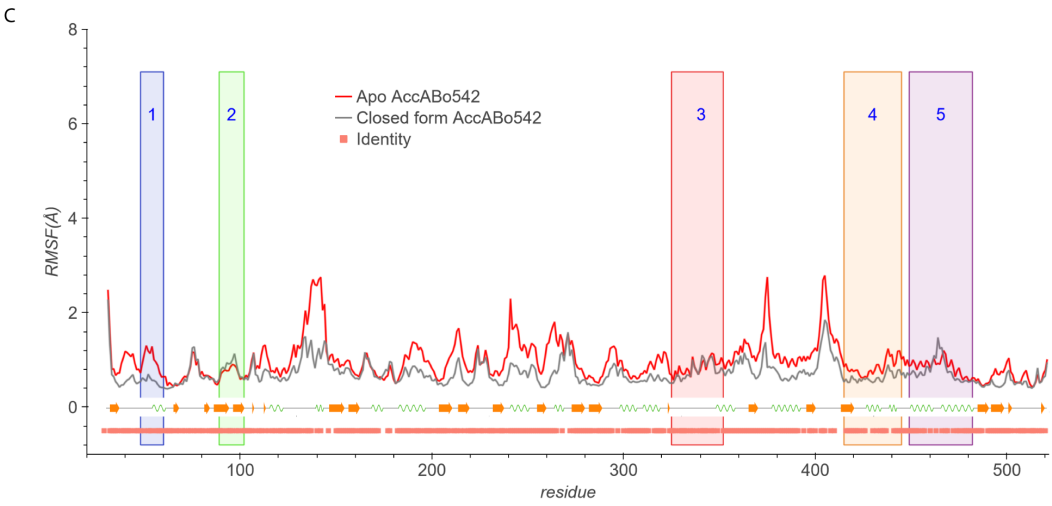
C
Apo AccABo542
Closed form AccABo542
Identity
RMSF(Å)
residue
1
2
3
4
5

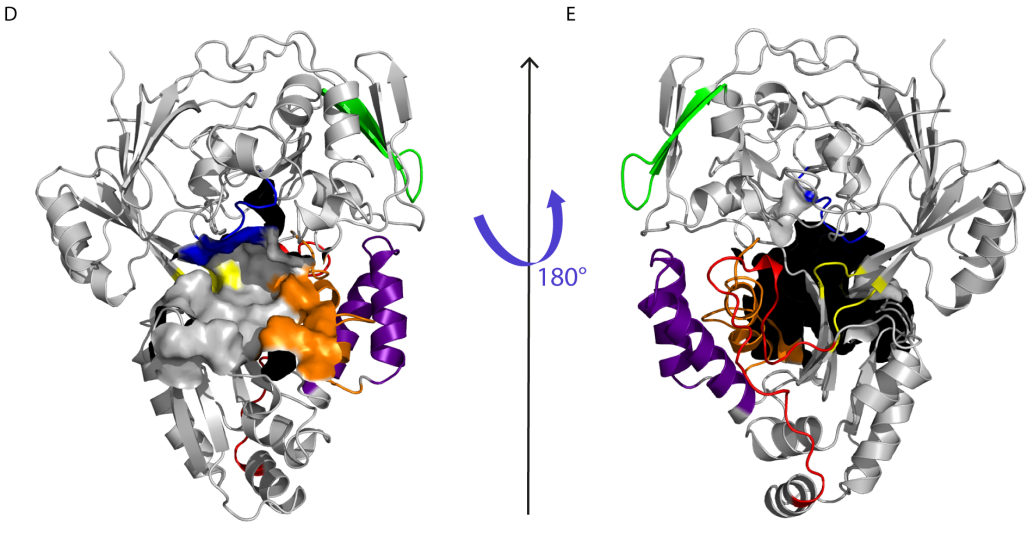
D
E
180°

A highly conserved ligand-binding site for AccA transporters of antibiotic and quorum-sensing regulator in *Agrobacterium* leads to a different specificity

Solange Moréra[1]*, Armelle Vigouroux[1], Magali Aumont-Nicaise[1], Mohammed Ahmar[2], Thibault Meyer[3], Abbas El Sahili[1$], Grégory Deicsics[1], Almudena González-Mula[1], Sizhe Li[2], Jeanne Doré[3], Serena Siragu[4], Pierre Legrand[4], Camille Penot[1], François André[1], Denis Faure[1], Laurent Soulère[2], Yves Queneau[2], Ludovic Vial[3]

[1]Université Paris-Saclay, CEA, CNRS, Institute for Integrative Biology of the Cell (I2BC), 91198, Gif-sur-Yvette, France

[2]Univ Lyon, Institut de Chimie et Biochimie Moléculaires et Supramoléculaires, CNRS, Université Lyon 1, INSA Lyon, CPE Lyon, ICBMS, UMR 5246; Université Claude Bernard, Bâtiment Lederer, 69622 Villeurbanne Cedex, France

[3]UMR Ecologie Microbienne, CNRS, INRAE, VetAgro Sup, UCBL, Université de Lyon, F-69622, Villeurbanne, Lyon, France

[4]Synchrotron SOLEIL, HelioBio group, 91190 Saint-Aubin, France

Short title: Specificity of the *Agrobacterium tumefaciens* strain Bo542 for agrocinopine uptake

*Corresponding author: solange.morera@i2bc.paris-saclay.fr; Tel +33 1 69 82 42 13, ORCID ID: 0000-0001-7781-0448

Table S1. Crystallographic data and refinement parameters for the liganded AccAC58

AccAC58	**agrocinopine D-like2**	**agrocinopine A**	**agrocinopine C-like3**
PDB code	**8CKD**	**8CKE**	**8CKO**
Crystallization conditions	A: 25% PEG 4K/0.2 M AcNH4/0.1 M Na Citrate pH 5.6	A	A
Space group Cell parameters (Å,°)	*I*222 *a* = 78.1 *b* = 108.2 *c* = 113.1	*I*222 *a* = 77.9 *b* = 108 *c* = 112.7	*I*222 *a* = 78.7 *b* = 108.9 *c* = 113.2
Resolution (Å)	42.2.-1.6 (1.71-1.6)	78-1.29 (1.44-1.3)	78-1.42 (1.53-1.42)
Estimated resolution limit (Å) STARANISO		1.3, 1.44, 1.67	1.42, 1.55, 1.53
No. of observed reflections	576191 (95140)	1080065 (57696)	1008813 (52198
No. of unique reflections	63379 (10139)	78672 (3936)	74582 (3729)
Completeness (%)	100 (99.9)	67.1 (12.2)	81.5 (19.9)
R_{merge} (%)	15 (136.6)	8.6 (160.7)	11.9 (205.9)
R_{pim} (%)	5.3 (46.6)	2.4 (43.3)	3.4 (57)
$I/\sigma(I)$	12.98 (1.57)	15.5 (1.6)	13.1 (1.5)
$CC_{1/2}$	0.998 (0.587)	0.999 (0.63)	0.999 (0.422)
R_{cryst} (%)	17.8	15.4	16.2
R_{free} (%)	20.4	18.7	19.5
rms bond deviation (Å)	0.01	0.01	0.01
rms angle deviation (°)	1	1.19	1.1
Average *B* (Å^2) Protein ligand solvent	 25.8 24.1 36.9	 19 17.3 30.6	 23.7 28.6 32.6
[a]Clashscore MolProbity score	0.37 0.9	0.88 0.95	0.5 0.88
[a]Ramachandran plot (%) Favored Outliers	 96.11 0	 96.93 0	 96.73 0

Values for the highest resolution shell are in parentheses.
$CC_{1/2}$= percentage of correlation between intensities from random half-dataset.
[a]Calculated with MolProbity
STARANISO applies ellipsoidal mask: estimated resolution limits along the three crystallographic directions *a**, *b**, *c**.

Table S2. Crystallographic data and refinement parameters for the liganded AccAS4

AccAS4	**D-glucose-2-phosphate**	**agrocinopine D-like2**	**L-arabinose-2-phosphate**	**agrocinopine A**	**agrocinopine C-like4**	**agrocin 84**
PDB code	**8CI6**	**8CHC**	**8CH2**	**8CH1**	**8CH3**	**8CJU**
Crystallization conditions	20% PEG 8K 0.1 M MES pH 6.5	C: 20% PEG8K 0.1 M Hepes pH 7	C	C	D:20% PEG8K 0.1 M Tris pH 7.5	D
Space group Cell parameters (Å,°)	$P2_12_12_1$ a = 47.3 b = 61.1 c = 152.5	$P2_12_12_1$ a = 47 b = 61 c = 151.5	$P2_12_12_1$ a = 47.1 b = 60 c = 152.8	$P2_12_12_1$ a = 47.1 b = 61.6 c = 151.3	$P2_12_12_1$ a = 46.8 b = 60 c = 151.4	$P2_12_12_1$ a = 47 b = 60.7 c = 151.9
Resolution (Å)	47.66-1.20 (1.27-1.2)	33.39-1.68 (1.78-1.68)	50-1.4 (1.49-1.4)	44.97-1.5 (1.59-1.50)	47.36-1.4 (1.48-1.4)	38.89-1.35 (1.43-1.35)
No. of observed reflections	1645347 (167102)	609872 (76638)	1137987 (182224)	833423 (125060)	1066837 (154873)	1255428 (178563)
No. of unique reflections	138637 (21841)	49148 (6588)	86791 (13746)	70531 (10968)	85091 (13395)	96419 (15219)
R_{sym} (%)	7.2 (88.1)	11.1 (159.1)	4.5 (41.2)	9 (130.3)	8.2 (236.4)	6.8 (106.5)
R_{pim} (%)	2.1 (33.1)	7.5 (37.3)	1.3 (11.6)	2.7 (39.5)	3.3 (115)	2.1 (59.4)
Completeness (%)	99.7 (98.2)	97.1 (81.9)	99.8 (99.1)	99.5 (97)	98.9 (97.5)	99.7 (98.4)
$I/\sigma(I)$	16.5 (1.6)	12.8 (1.2)	30.6 (5.7)	14.9 (1.5)	14.2 (1)	16.8 (2.1)
$CC_{1/2}$	0.99 (0.70)	0.99 (0.77)	1 (0.96)	0.99 (0.97)	0.99 (0.45)	0.99 (0.83)
R_{cryst} (%)	17.8	19.5	17.3	17.4	19	21.8
R_{free} (%)	19.7	21.9	19.2	20.2	21.8	24.4
rms bond lengths (Å)	0.01	0.009	0.01	0.01	0.01	0.01
rms bond angles (°)	1.06	1.05	1.16	1.10	1.13	1.2
Average B (Å^2)						
Protein	23.7	39.8	25.9	27.2	32.9	28.8
Ligand	17.6	38.7	20.9	23.8	35.6	43.6
Solvent	32.8	40.3	32.6	34.9	36.7	34.5
Clashscore[a]	1.04	1.18	0.78	0.91	1.95	1.94
MolProbity score[a]	0.93	1.04	0.85	0.84	1.22	1.24
Ramachandran plot (%)						
Favored	97.5	97.3	97.48	97.7	96.9	96.64
Outliers	0	0	0	0	0	0

Values for the highest resolution shell are in parentheses.

$CC_{1/2}$ = percentage of correlation between intensities from random half-dataset.

[a]Calculated with MolProbity

Figure S1. **Scheme of the synthesis of agrocinopine C-like2 and analogues of agrocinopine C-like2.** Analogues were obtained from the synthesis namely AgroC-like1', AgroC-like3 and AgroC-like4. (**A**). Mass spectra of the synthesized agrocinopine C-like2. The expected molecular weight was 583 Da and the measured peak corresponds to 583.16 ± 0.1 Da (**B**).

A

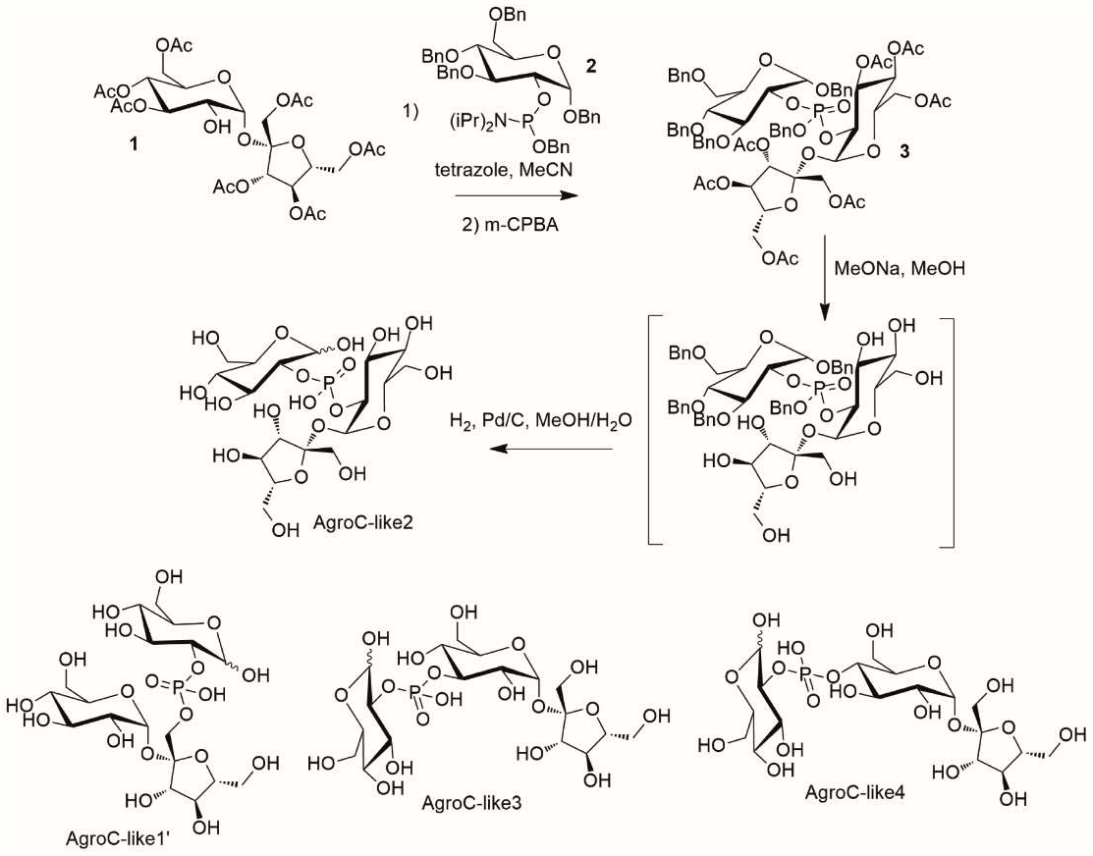

B

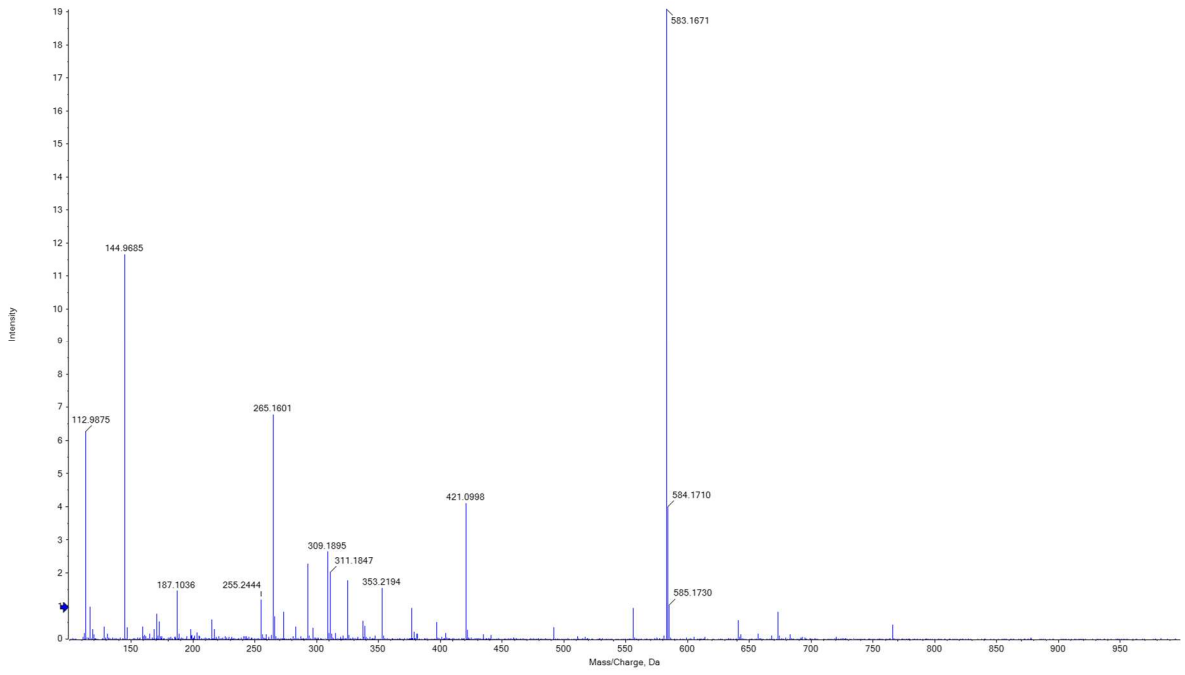

Figure S2. Differential scanning calorimetry thermograms of AccABo542 (A) and AccAC58 (B), without and with different agrocinopines and derivatives.

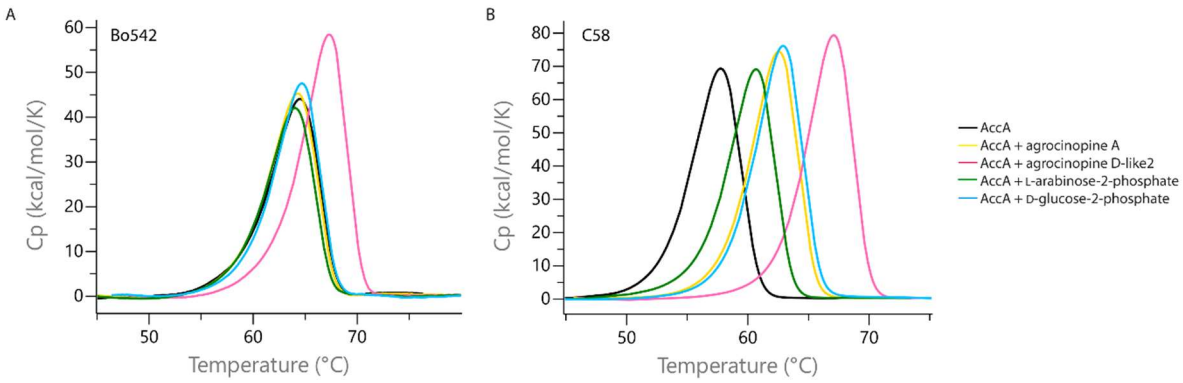

Figure S3. Effect of agrocinopines and derivatives presence on the thermal unfolding of AccABo542 (A) and AccAC58 (B), measured by nanoDSF on a Tycho NT.6 instrument.

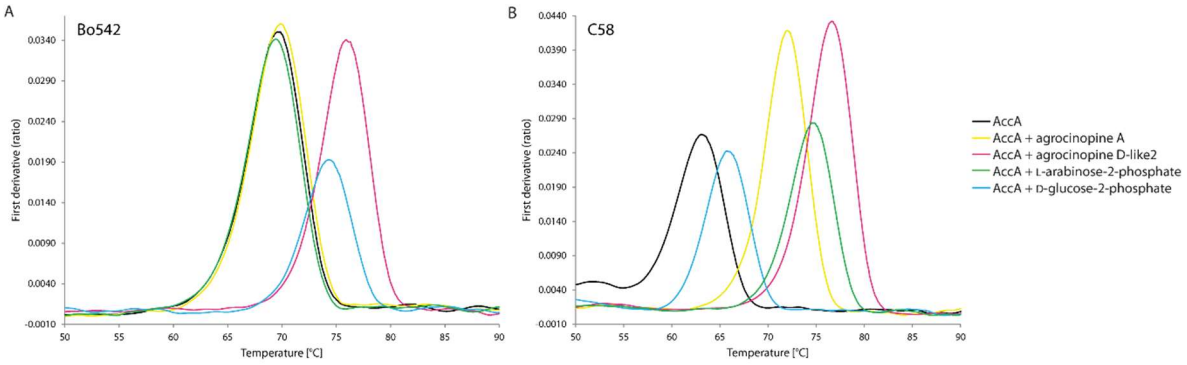

Figure S4. Fluorescence experiments and isothermal titration microcalorimetry: K_D measurements of AccABo542 (**A**) and AccAC58 (**B**) towards D-glucose-2-phosphate and agrocinopine D-like2. The top panels show fluorescence monitoring of each protein upon titration with each ligand and fit (solid line) to a single binding model using Origin 7. The medium panels show heat differences upon injection of ligand and the low panels show integrated heats of injection with the best fit (solid line) to a single binding model using Microcal ORIGIN. ITC experiments were performed twice and fluorescence were done on triplicate.

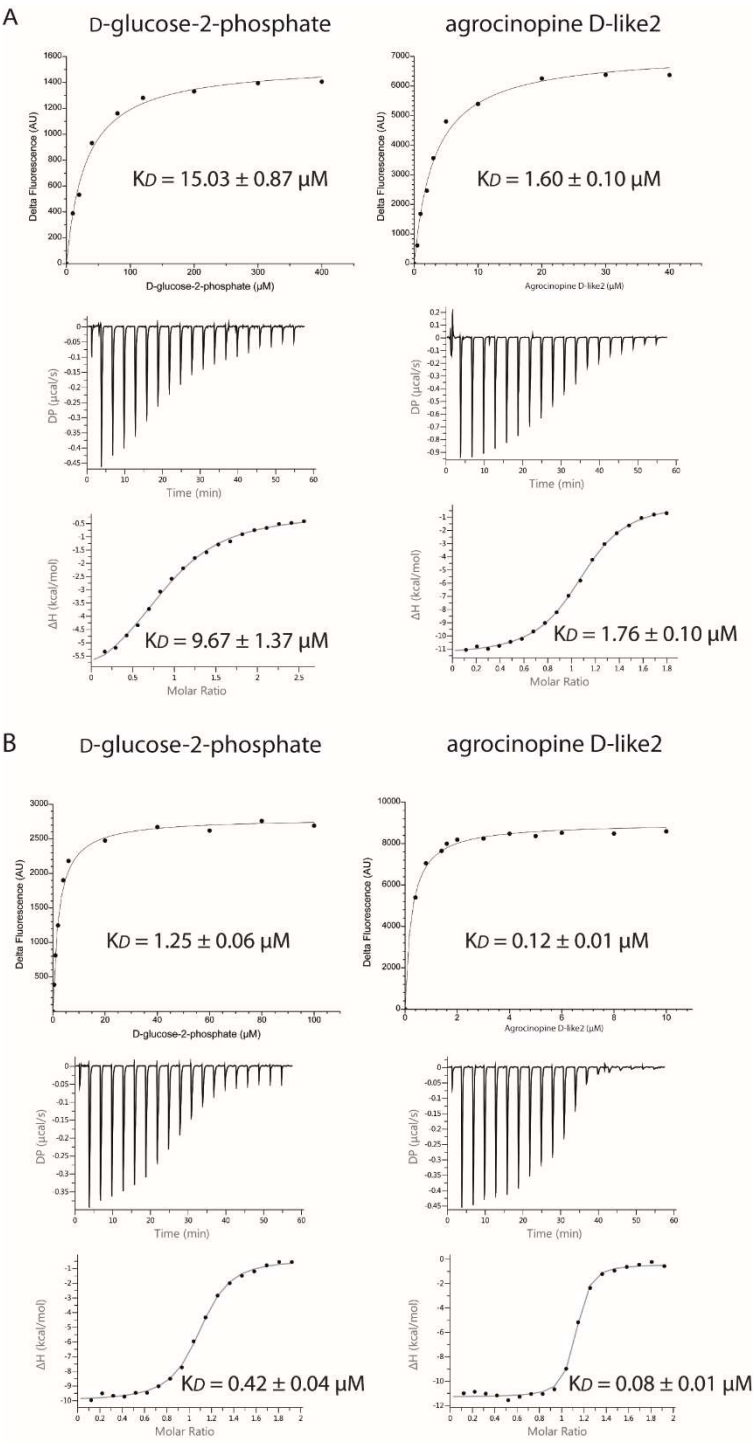

Figure S5. D-glucose-2-phosphate anomers (in blue) bound to AccABo542 (in cyan). Hydrogen bonds are shown as dashed lines in black and red, for distances up to 3.2 Å and 3.4 Å, respectively. (**A**) alpha anomer for the OH1 group of glucose, (**B**) beta anomer for the OH1 group of glucose.

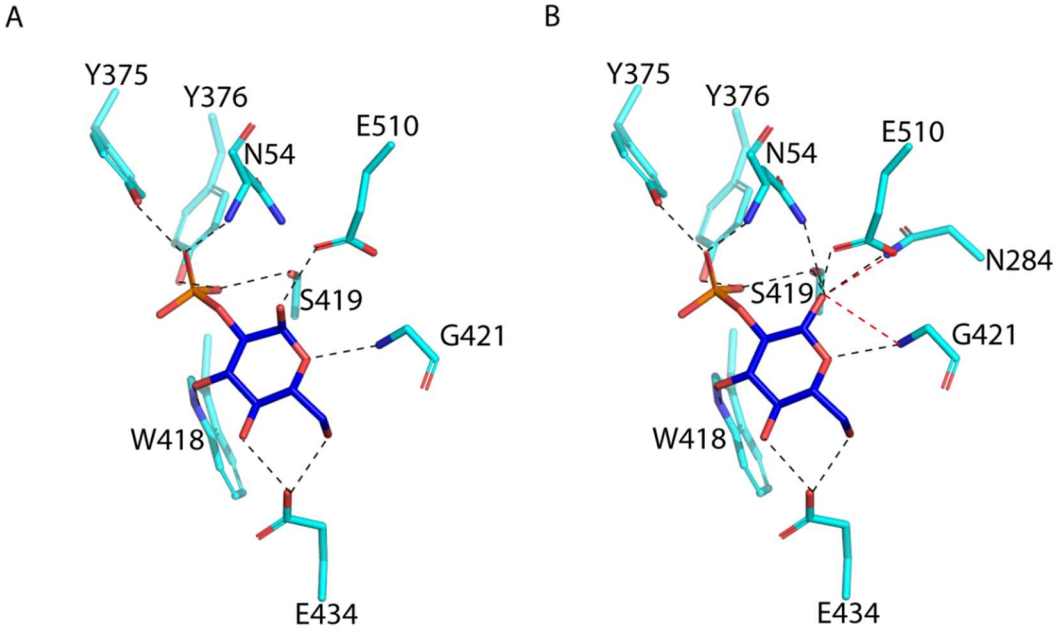

Figure S6. Superposition of agocinopine A bound to AccAC58 from the highest resolution structure of this study (PDB 8CKE, in yellow) and in the previous published structure (PDB 4ZEB, in pink). Alpha and beta anomers for the arabinose OH1 group are well defined in the *Fo-Fc* omit map contoured at 4σ. Glc, Rib, P and Ara labels are for Glucose, Ribose, Phosphate and Arabinose, respectively (**A**). Interaction between agrocinopine A in yellow and AccAC58 (PDB 8CKE) amino-acids in pink. Hydrogen bonds are shown as dashed lines in black and red, for distances up to 3.2 Å and 3.4 Å, respectively (**B**).

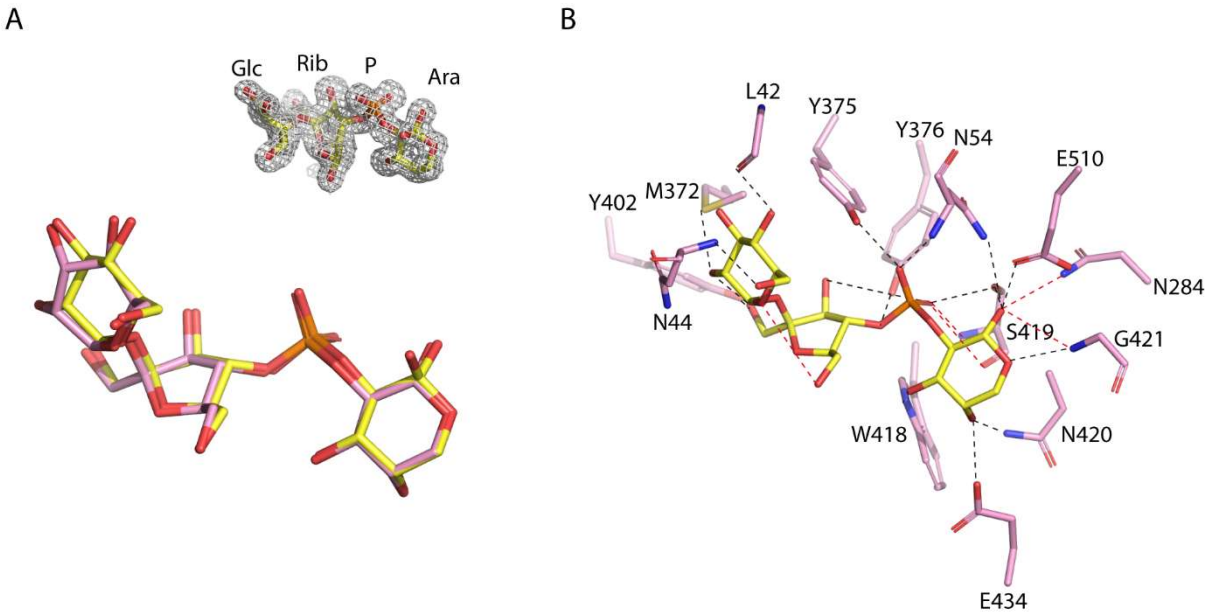

Figure S7. **Effect of agrocinopine and derivatives on AccAS4**. (**A**) Measurement by nanoDSF on a Tycho NT.6 instrument. The table indicates the *Ti*. NanoDSF experiments were performed twice. (**B**) K_D measurements of AccAS4 towards ligands by fluorescence experiments. The fluorescence monitoring of each protein upon titration with each ligand and fit (solid line) to a single binding model using Origin 7. Fluorescence were performed on triplicate.

A

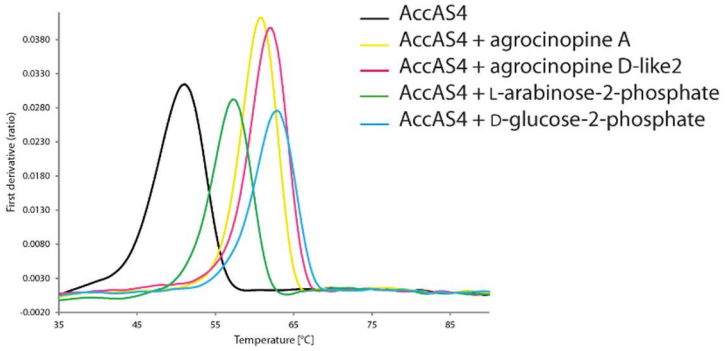

AccAS4	*Ti* (°C)	*ΔTi* (°C)	Initial Ratio	ΔRatio
Apo	51.01 ± 0.15		0.6972	0.3070
agrocinopine A	60.78 ± 0.01	**9.8**	0.7130	0.2914
agrocinopine D-like2	61.98 ± 0.43	**11**	0.6954	0.3081
L-arabinose-2-phophate	57.27 ± 0.29	**6.3**	0.7709	0.2267
D-glucose-2-phospahe	62.87 ± 0.56	**11.9**	0.7660	0.2395

B

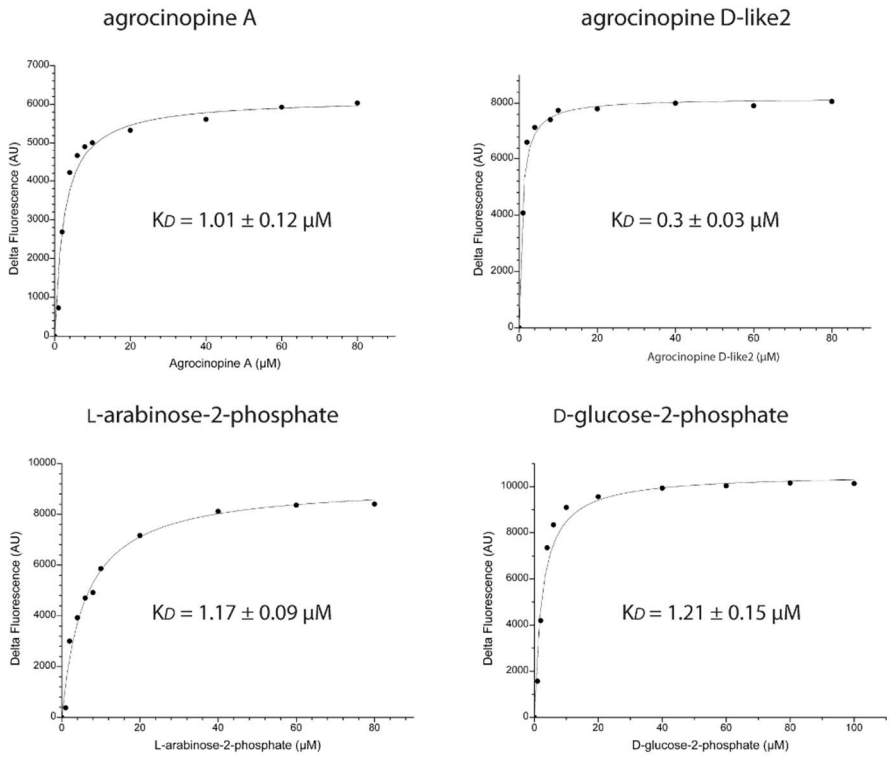

Figure S8. **Ligand binding site of AccAS4**. Amino acids involved in the ligand binding are shown as stick. Hydrogen bonds are shown as dashed lines in black and red for distances up to 3.2 Å and 3.4 Å, respectively. (**A**) L-arabinose-2-phosphate in green, (**B**) agrocinopine A in yellow, (**C**) D-glucose-2-phosphate in blue, (**D**) agrocinopine D-like2 in hot pink, and (**E**) agrocin 84 in orange. Each ligand is shown in its Fo-Fc omit map contoured at 4σ. Glc, Rib, P, Ara and TM84 labels are for Glucose, Ribose, Phosphate, Arabinose and Toxic Moiety 84, respectively.

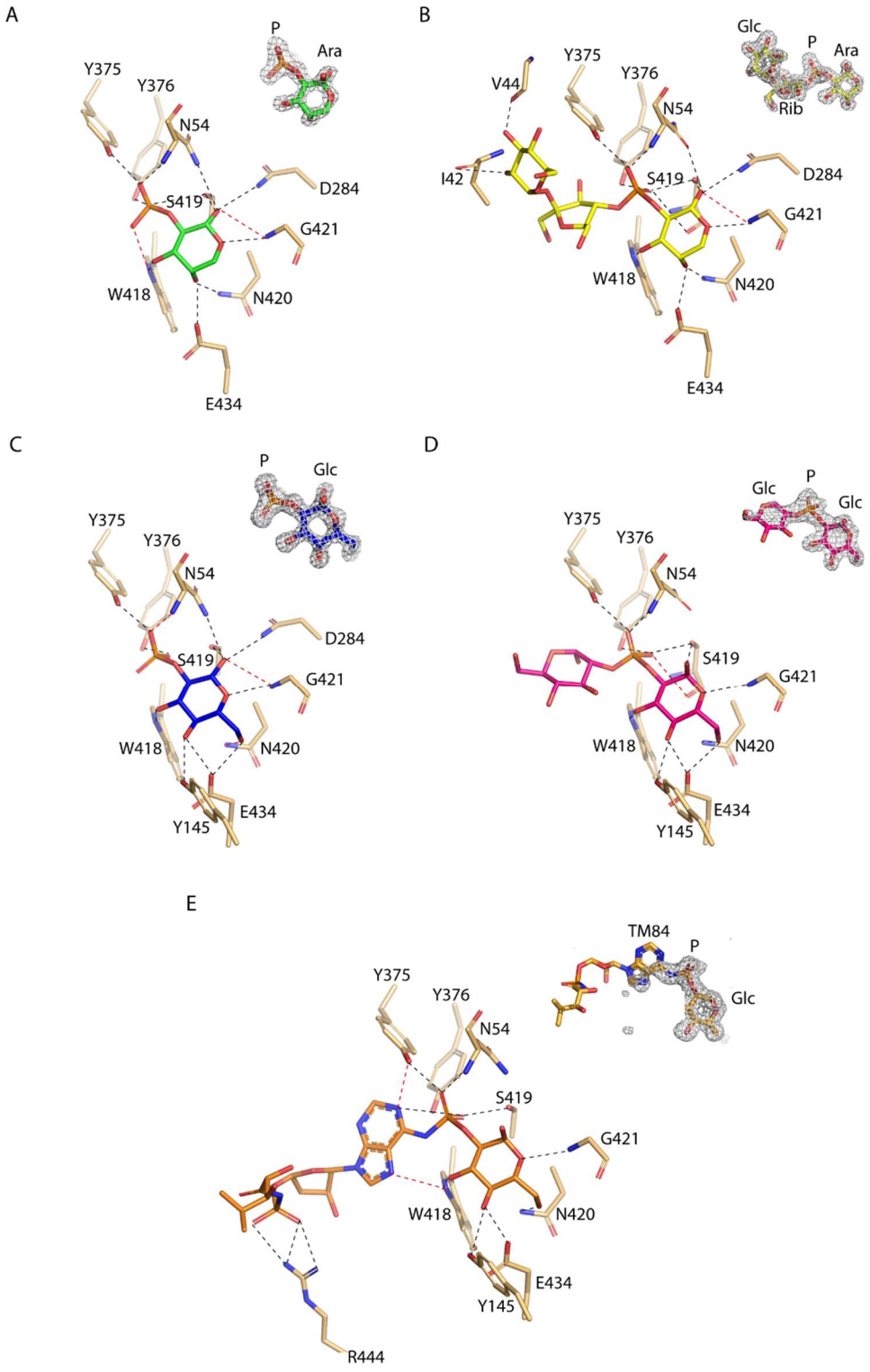

Figure S9. Growth assays and gene expression. (**A**) Growth comparison of *A. vitis* S4 strain measured in AB minimal medium supplemented with succinate (orange), agrocinopine D-like2 (pink), L-arabinose-2-phosphate (green), D-glucose-2-phosphate (blue), used as carbon sources. Results are the average of three independent experiments. (**B**) Expression of the *accA* gene in *A. fabrum C58* and *A. vitis S4* strains. P*accA*C58 and P*accA*S4 expression were compared after 20 hours in AB minimal medium containing succinate (in black) supplemented or not with L-arabinose-2-phosphate (A2P, in gray). Growth curves correspond to the mean from two biological replicates and four technical replicates.

A

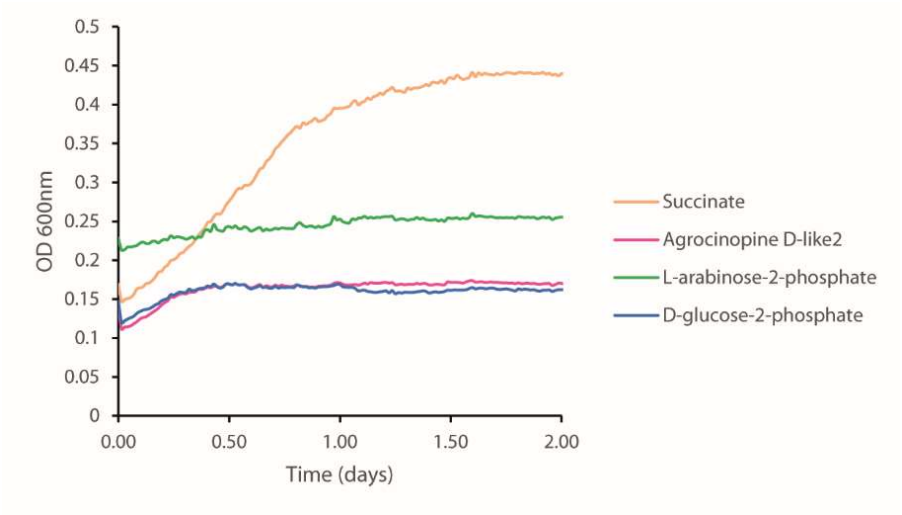

B

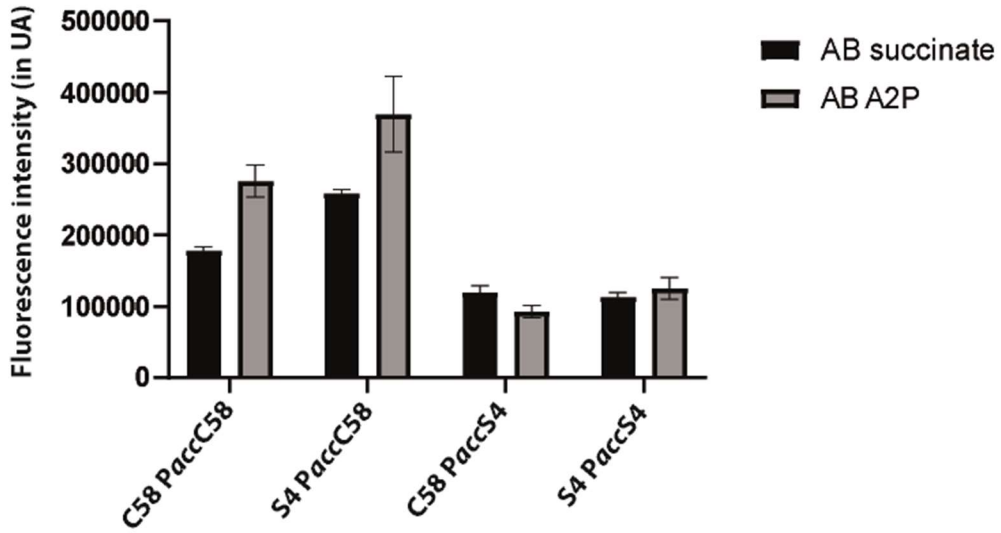

Figure S10. **AccABo542F145YG440Q mutant**. (**A**) Superposition of the ribbon representation of apo AccABo542 (in cyan, PDB 8C6R) and apo AccABo542F145YG440Q (in orange, PDB 8C6U). Phe/Tyr145 and Gln/Gly440 are shown in sticks. (**B**) Effect of agrocinopine and derivatives on AccABo542F145YG440Q measured by differential scanning calorimetry and (**C**) nanoDSF on a Tycho NT.6 instrument. The table below indicates the *Tm* and *Ti*. DSC and NanoDSF experiments were performed twice. (**D**) K_D measurements of AccABo542F145YG440Q for G2P by autofluorescence experiments, done on triplicate.

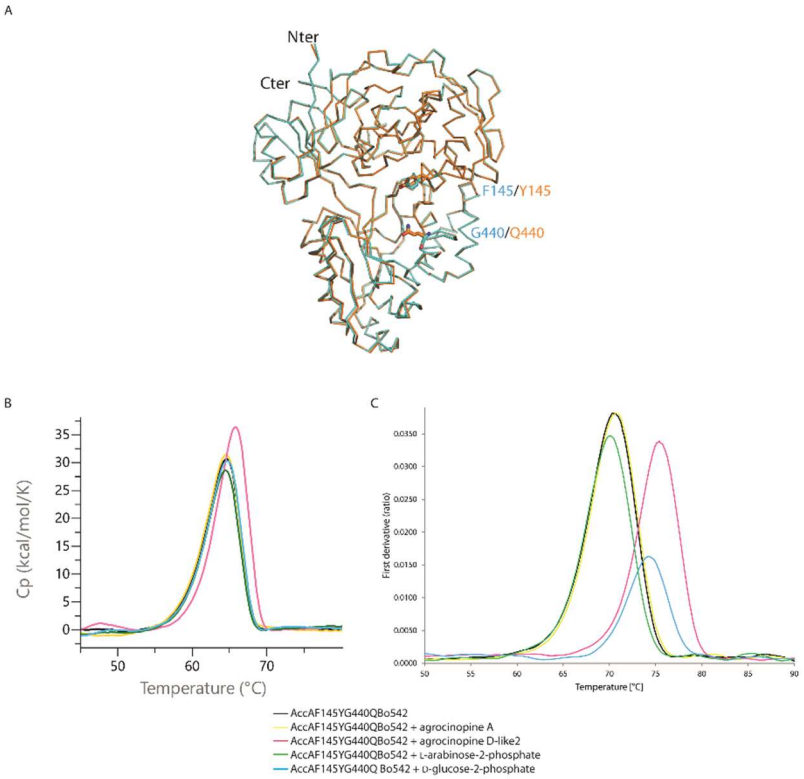

AccABo542 F145YG440	*Tm* (°C)	*ΔTm* (°C)	ΔH_1 (kcal/mol)	ΔHVH_1 (kcal/mol)	*Ti* (°C)	*ΔTi* (°C)	Initial Ratio	ΔRatio
Apo	63.97 ± 0.01		178	156	70.54 ± 0.03		0.7520	0.2904
agrocinopine A	63.89 ± 0.01	**-0.08**	184	154	70.69 ± 0.05	**0.2**	0.7626	0.2858
agrocinopine D-like2	65.20 ± 0.009	**1.23**	197	168	75.36 ± 0.18	**4.9**	0.7976	0.2461
L-arabinose-2-phophate	63.86 ± 0.009	**-0.11**	161	161	69.97 ± 0.31	**-0.5**	0.7719	0.2603
D-glucose-2-phospahe	64.06 ± 0.01	**0.09**	175	157	74.22 ± 0.26	**3.7**	0.8983	0.1477

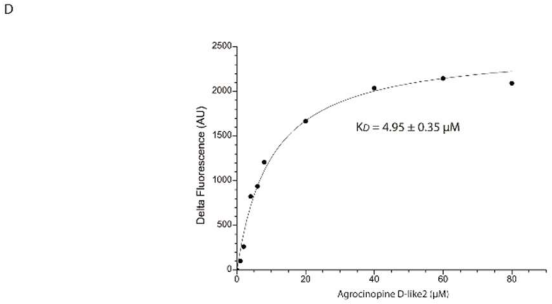

Figure S11. **Molecular dynamics simulation**. RMSD along the molecular dynamics of apo AccAC58 (in blue, PDB 4ZE8), apo AccABo542 (in red, PDB 8C75), the closed form of AccAC58 (in orange, PDB 8CKD) and the closed form of AccABo548 (in grey, PDB 8CAY) (**A**). RMSF comparison between the closed forms of AccAC58 and AccABo542, colored boxes are referred in Figure 10 of the manuscript (**B**).

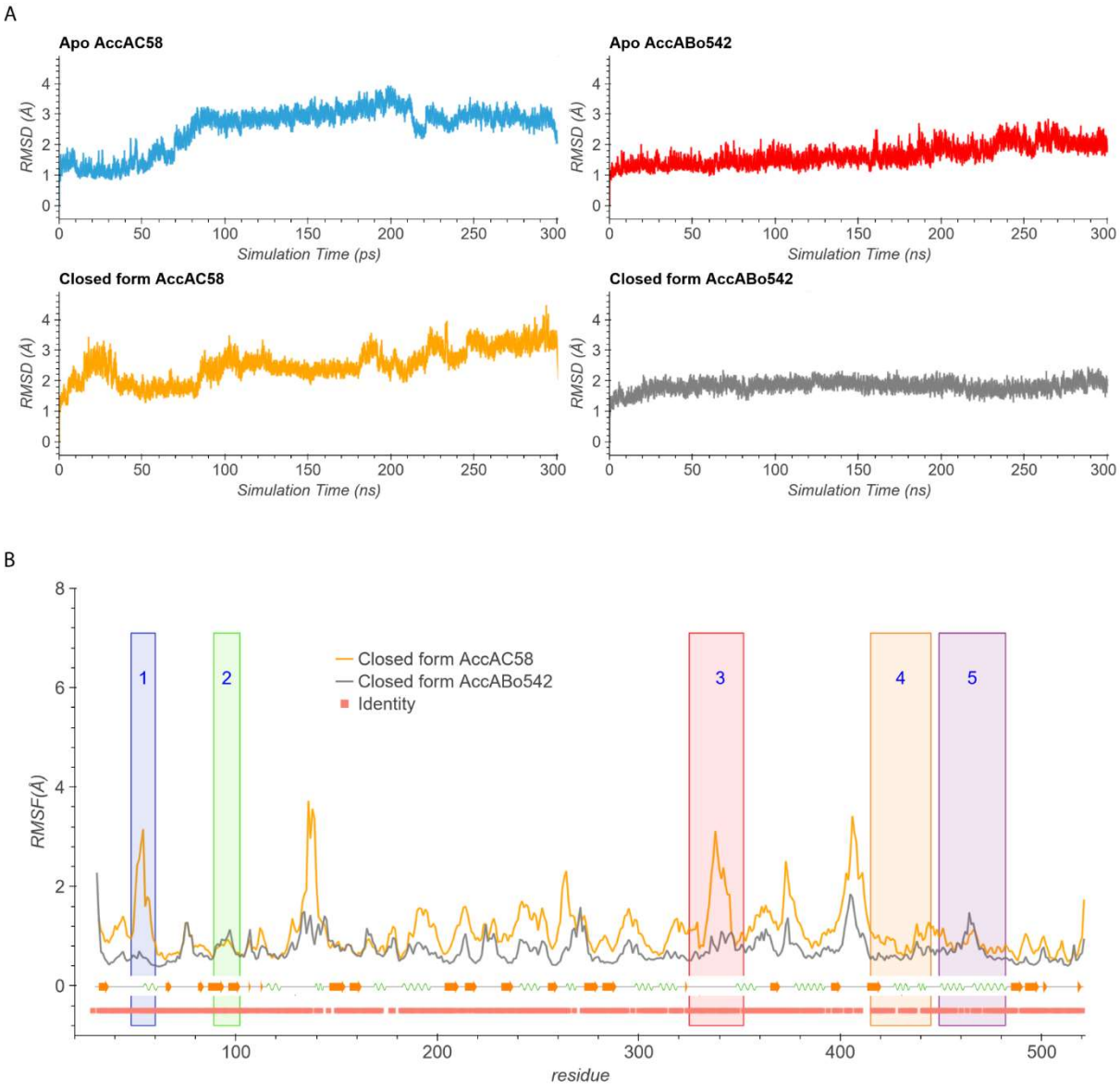

Supplementary information for AgroC-like2 synthesis referring to Figure S1

3,4,6,3',4',6'-Hexa-*O*-acetyl-1'-*O*-acetylsucrose (**1**) was synthesized according to the method reported by F. W. Lichtenthaler and co-workers from sucrose which was benzylated in position 2, peracetylated and lastly debenzylated affording compound **1** (F. W. Lichtenthaler, S. Immel, P. Pokinskyj, Liebigs Ann. 1995, 1939–1947). Diisopropylphosphoramidite **2** was prepared following similar procedures as those reported in (El Sahili *et al.*, PLOS Pathogen 2015, 11, e1005071).

Benzyl ((2S,3R,4S,5R,6R)-2,4,5-tris(benzyloxy)-6-((benzyloxy)methyl)tetrahydro-2H-pyran-3-yl) diisopropylphosphoramidite (**2**): The tetrazole salt catalyst was prepared by stirring tetrazole (519 µL, 0.6 eq, 0.2334 mmol, 0.45 M in CH_3CN), diisopropylamine (40 µL, 0.7 eq, 0.2723 mmol) in anhydrous CH_2Cl_2 (1 mL) for 10 min at room temperature before evaporation leading to a white solid. This tetrazole salt was added to a solution of benzyl 3,4,6-tri-*O*-benzyl-α-D-glucopyranoside (210 mg, 0.389 mmol) in 5 mL of dichloromethane and benzyloxy-bis(diisopropylamino)phosphine (200 mg, 0.583 mmol). The mixture was dried by co-evaporation with toluene three times before dichloromethane was added. The reaction was then stirred for 18 h from 0°C to room temperature until the starting material was fully consumed. Then the mixture was diluted in 15 mL of dichloromethane and washed with saturated $NaHCO_3$ and brine (20 mL respectively). The organic layer was separated, dried over anhydrous Na_2SO_4, concentrated and purified by flash column chromatography (pentane/AcOEt=13/1 with 1% triethylamine) to afford 230 mg of product **2** as a colorless oil (73% yield). ^{1}H NMR (300 MHz, Chloroform-d) δ: 7.40 – 7.20 (m, 23H, ArH), 7.08 (dd, J = 6.8, 2.9 Hz, 2H, ArH), 5.14 (d, J = 3.6 Hz, 1H, H-1), 4.83 – 4.40 (m, 10H, $PhCH_2$), 4.13 (q, J = 7.1 Hz, 1H, H-5), 4.04 – 3.96 (m, 1H, H-2), 3.92 – 3.83 (m, 2H, H-6, H-3), 3.67 (m, 4H, H-6, H-4, 2CH), 1.14 (t, J = 6.7 Hz, 12H, 4 CH3). ^{31}P NMR (122 MHz, Chloroform-d) δ 149.94, 148.80. HRMS m/z (ESI): Calcd. for $C_{47}H_{56}NO_7P$ (M+H)+ : 778.3873. Found: 778.3.

(Benzyl 3,4,6-tri-*O*-benzyl-α-D-glucopyranoside-2-yl)-(3,4,6,3',4',6'-hexa-*O*-acetyl-1'-*O*-acetylsucrose-2-yl) benzylphosphate (**3**): To a solution of 3,4,6,3',4',6'-hexa-*O*-acetyl-1'-*O*-acetylsucrose (**1**) (232 mg, 0.364 mmol), benzyl 3,4,6-tri-O-benzyl-α-D-glucopyranoside diisopropylphosphoramidite (**2**) (340 mg, 0.437 mmol), 1H-tetrazole (0.40 mmol, 890 µl, 0.45 M in CH_3CN) was added at room temperature. The reaction was stirred at the same temperature for 6 h until the sucrose derivatives was consumed. Then the m-CPBA (0.168 mmol, 30 mg) was added at 0°C and stirred for 2 h at room temperature. After purification by flash chromatography (pentane/AcOEt=1/1), 168 mg (35% yield) of the desired product was obtained as a white solid. ^{1}H NMR (400 MHz, Chloroform-d) δ: 7.40 – 7.21 (m, 23H, Bn), 7.10 (dd, J = 6.7, 2.9 Hz, 2H, Bn), 5.75 (d, J = 3.7 Hz, 1H, G1), 5.53 – 5.37 (m, 2H, F3 and F4), 5.27 (dd, J = 8.8, 3.6 Hz, 1H, G3), 5.12 – 4.91 (m, 2H, G4, G'1), 4.83 – 4.66 (m, 4H, 2Bn), 4.63 – 4.42 (m, 7H, G2, 3Bn), 4.37 – 4.07 (m, 10H, G'2, G5, G6, F1, F5, F6, G'3), 3.81 (d, J = 6.9 Hz, 1H, G'6), 3.76 – 3.54 (m, 3H, G'6, G'4, G'5), 2.10 (s, 3H, Ac), 2.08 (s, 3H, Ac), 2.07 (s, 3H, Ac), 2.06 (s, 3H, Ac), 2.04 (s, 3H, Ac), 2.03 (s, 3H, Ac), 1.92 (s, 3H, Ac). ^{13}C NMR (101 MHz, Chloroform-d) δ: 170.7 (CO), 170.5 (CO), 170.3 (CO), 169.9 (CO), 169.8 (CO), 169.8

(CO), 169.4 (CO), 138.2 (ArC), 138.1 (d, J = 3.3 Hz, ArC), 137.9 (ArC), 137.9 (ArC), 137.0 (ArC), 128.5 (ArC), 128.5 (ArC), 128.4 (ArC), 128.4 (ArC), 128.3 (ArC), 128.2 (ArC), 128.1 (ArC), 128.00 (ArC), 127.9 (ArC), 127.8 (ArC), 127.7 (ArC), 103.4 (F-C2), 96.6 (G'-C1), 90.2 (d, J = 2.1 Hz, G-C1), 80.6 (d, J = 6.8 Hz, G'-C3), 78.4 (F-C5), 77.7 (G'-C4), 77.3 (G'-C2), 75.5 (OBn), 75.3 (OBn), 75.1 (F-C4), 74.1 (F-C3), 73.9 (G-C3), 73.5 (OBn), 70.5 (G'-C5), 70.3 (OBn), 69.9 (d, J = 5.6 Hz, GC2), 68.4 (G-C4), 68.2 (G'-C6, G-C5), 63.4 (F-C6), 63.2 (F-C1), 61.9 (G-C6), 61.5 (d, J = 5.4 Hz, OBn), 20.8 (Ac), 20.7 (2Ac), 20.6 (Ac), 20.5 (2Ac), 20.4 (Ac). (G=glucose part of sucrose, G'=glucose). ^{31}P NMR (162 MHz, Chloroform-d) δ: -0.65 – -0.92 (m), -1.54 (p, J = 7.2 Hz). HRMS m/z (ESI): Calcd. for $C_{67}H_{77}O_{26}NaP$ $[M+Na]^+$: 1351.4338. Found: 1351.4333. [α]D = +33.0 (c 1.0, $CHCl_3$).

AgroC-like2 sucrose ammonium salt: Compound **3** (40 mg, 0.0301 mmol) were treated with fresh 0.1 M CH_3ONa solution in methanol (5 mL, 5 mL respectively) at room temperature.A large amount of salt was emerged, and the reaction was monitored by TLC (AcOEt/CH_3COOH/CH_3OH/H_2O=9/3/3/2) until the sucrose derivatives were consumed (5 h). Then a spatula of Dowex 50 (H^+) was added, and the mixture was allowed to stir at room temperature for 5 min, and filtered. The filtrate was evaporated in vacuo to give a white solid as crude product. The structure of the intermediate was confirmed by ^{1}H-NMR and mass spectroscopy (ESI: Calcd. for $C_{53}H_{63}O_{19}NaP$ $[M+Na]^+$: 1057.36. Found: 1057.40) and was used for the next step directly. The obtained products were dissolved in 5 mL methanol and water (v/v, 1/1), and treated with Pd/C (20 mg, 20 mg respectively) under hydrogen atmosphere for 14 h. The Pd/C was filtered through a celite layer and the filtrate was concentrated and purified on a C18 column and ion exchange chromatography on a DEAE-Sephadex column eluted with NH_4CO_3 to afford AgroC-like2 sucrose ammonium salt as a white solid (10 mg, 53%; 15 mg, 79%). ^{1}H NMR (500 MHz, Deuterium Oxide) δ: 5.45 (d, J = 3.7 Hz, 2H, G1, G'1), 4.39 (q, J = 8.4, 7.9 Hz, 1H, F4), 4.21 (dd, J = 8.8, 2.4 Hz, 1H, F3), 4.09 – 3.95 (m, 4H, G'2, F6, G3), 3.92 – 3.73 (m, 6H, G'3, G6, F5, G5, G'5), 3.70 –3.69 (dt, J = 9.5, 5.3 Hz, 5H, G2, F1, G'6), 3.51 – 3.44 (m, 2H, G'4, G4). ^{13}C NMR (101 MHz, Deuterium Oxide) δ: 103.7 (F-C2), 92.1 (G'-C1), 90.8 (G-C1), 81.3 (F-C4), 78.5 (F-C5), 76.5 (d, J = 5.0 Hz, G-C2), 75.9 (F-C3), 74.4 (G-C3), 74.1 (G-C5), 74.0 (G'-C3), 72.1 (G'-C4), 71.6 (G'-C5), 71.3 (d, J = 4.5 Hz, G'-C2), 69.4 (G-C4), 62.3 (F-C6), 61.3 (F-C1), 60.5 (G-C6), 60.0 (G'-C6). ^{31}P NMR (202 MHz, Deuterium Oxide) δ: 0.06 – -0.49 (m), -0.62 – -0.97 (m). HRMS m/z (ESI): Calcd. for $C_{18}H_{32}O_{19}P$ $[M-H]^-$: 583.1281. Found: 583.1273. [α]D = +49.6 (c 1.0, H2O).